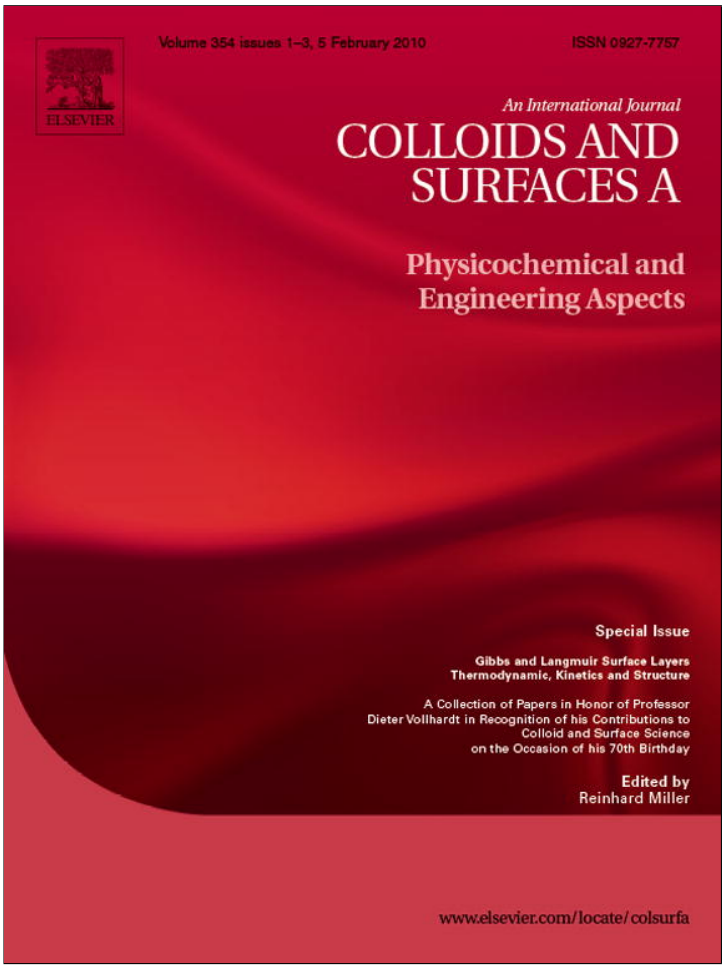

Colloids and Surfaces A: Physicochem. Eng. Aspects 354 (2010) 172–187

Contents lists available at ScienceDirect

Colloids and Surfaces A: Physicochemical and Engineering Aspects

journal homepage: www.elsevier.com/locate/colsurfa

Coexistence of micelles and crystallites in solutions of potassium myristate: Soft matter vs. solid matter

Mariana P. Boneva [a], Krassimir D. Danov [a], Peter A. Kralchevsky [a,*], Stefka D. Kralchevska [a], Kavssery P. Ananthapadmanabhan [b], Alex Lips [c]

[a] Laboratory of Chemical Physics & Engineering, Faculty of Chemistry, Sofia University, 1 James Bourchier Boulevard, Sofia 1164, Bulgaria
[b] Unilever Research & Development, 40 Merritt Boulevard, Trumbull, CT 06611, USA
[c] Unilever Research & Development, Port Sunlight, Quarry Road, East Bebington, Wirral CH63 3JW, UK

ARTICLE INFO

Article history:
Received 15 May 2009
Received in revised form 20 June 2009
Accepted 22 June 2009
Available online 30 June 2009

Dedicated to Professor Dieter Vollhardt (MPI–Potsdam/Golm) on the occasion of his 70th birthday.

Keywords:
Acid soaps
Carboxylate solutions
Fatty acid
Myristic acid
Microcrystalline precipitates
Surface tension isotherms

ABSTRACT

Here, we investigate the coexistence of surfactant micelles and acid-soap crystallites in solutions of potassium myristate (*n*-tetradecanoate) to determine the micelle composition and charge, and the stoichiometry of the acid soaps. We carried out parallel pH, conductivity, and solubilization measurements, which indicate that micelles are present in the potassium myristate solutions at the higher concentrations, in contrast with the results for sodium myristate, where no micelles were detected at room temperature. Theoretical expressions describing the concentration dependences of conductivity and pH of the micellar carboxylate solutions are derived. Diagrams, showing the concentrations of all species in the solution, are constructed. The comparison of theory and experiment indicates that the undissociated fatty acid is incorporated in acid-soap crystallites, i.e. it behaves as initiator of crystallization. The rest of dissolved carboxylate forms micelles that are composed only of carboxylate anions and bound potassium counterions. Above 2–3 times the critical micellization concentration (CMC), the main mass of the carboxylate is in micellar form, despite the presence of coexisting acid-soap crystallites. Surface tension isotherms are obtained and interpreted on the basis of the results for the bulk composition. The adsorption layer is composed mostly of fatty acid and 1:1 acid-soap molecules. Not only the appearance of micelles, but also the change in the stoichiometry of the acid soaps in the solution leads to kinks, and even jumps, in the surface tension isotherm. The results for acid-soap stoichiometry have been confirmed by independent analysis of crystals collected from the solutions.

1. Introduction

Potassium and sodium carboxylates with 12–18 carbon atoms, i.e. laurates (C_{12}), myristates (C_{14}), palmitates (C_{16}) and stearates (C_{18}), have found broad applications in personal-care and household detergency: in soap bars; cleaning products; cosmetics; facial cleaners; shaving creams and deodorants [1–3]. As known, the aqueous solutions of such carboxylate soaps are turbid because of the light scattering from micrometer-sized crystallites. The reason for the appearance of crystallites in these solutions is the spontaneous protonation of the carboxylate anion and the formation of undissociated fatty acid [4]:

$$Z^- + H_2O \leftrightarrow HZ + OH^- \quad (1.1)$$

Here and hereafter, we are using the notations in the basic paper by Lucassen [4], viz. Z^- is the carboxylate anion, and HZ is undissociated carboxylic (fatty) acid. The carboxylic acids with 12 and more carbon atoms have very low solubility in water. For this reason, their production in the above reaction leads to the precipitation of HZ micro-crystallites. The release of OH^- anions in this reaction leads to the increase in the solution's pH. At higher carboxylate concentrations, the fatty acid initiates the formation of acid-soap complexes [5–16]:

$$jHZ + nZ^- + nM^+ \leftrightarrow (HZ)_j(MZ)_n \quad (1.2)$$

where M^+ is the metal counterion (K^+ or Na^+). At room temperature, the acid-soap molecules are insoluble in water, so they also form crystallites. The physical reason for the appearance of acid-soap complexes is the formation of a hydrogen bond between the fatty acid (HZ) and neutral soap (MZ) molecules [9–14]. The formation of 1:1 acid soap, $(HZ)_1(MZ)_1$, seems to be the most natural result of precipitation. However, the experiments show that the acid-soap crystallites can have different stoichiometry: j:n = 1:1; 1:2; 2:1; 3:2, 4:1, etc. [3,9–11,15–17].

The spontaneous formation of fatty acid (HZ) molecules in the carboxylate solutions has one additional consequence: HZ adsorbs

* Corresponding author. Tel.: +359 2 8161262; fax: +359 2 9625643.
E-mail address: pk@lcpe.uni-sofia.bg (P.A. Kralchevsky).

0927-7757/$ – see front matter © 2009 Elsevier B.V. All rights reserved.
doi:10.1016/j.colsurfa.2009.06.031

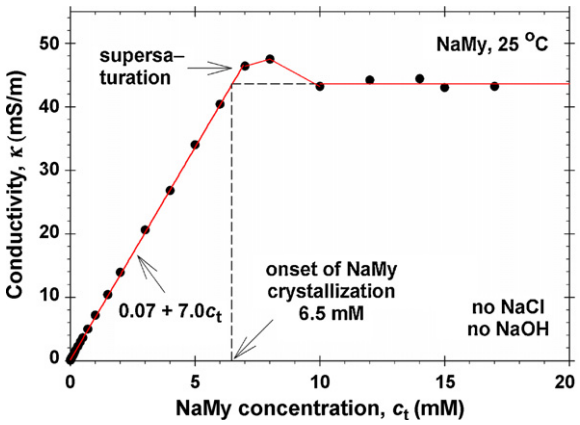

Fig. 1. Plot of the electrolytic conductivity, κ, vs. the total concentration, c_t, of NaMy solutions. In the zone without NaMy crystallites, the conductivity increases linearly with c_t. In the zone of two-phase precipitate, NaMy + 1:1 acid-soap, the conductivity levels off. The "horn" of the graph is due to supersaturation. The extrapolation of the plateau (the dashed line) gives the threshold concentration for MZ precipitation: $c_t \approx 6.5$ mM.

at the solution's surface, where it forms clusters [18,19] and causes surface phase transitions [20–23]. For this reason, HZ strongly enhances the surface rheology, as well as the rheology of the foams formed from carboxylate solutions, which has found applications for the production of foams with finely dispersed bubbles [24,25].

In a preceding paper [17], we investigated solutions of sodium laurate (NaL) and sodium myristate (NaMy) and developed a method for investigation of the stoichiometry of the acid soaps formed in these solutions at various concentrations by analysis of pH data. For example, at 25 °C and at the lowest concentrations of NaMy we detected the formation of HZ crystallites; at higher NaMy concentrations, we observed the consecutive formation of 4:1 and 1:1 acid soaps. Finally, at the highest concentrations, the 1:1 acid-soap crystallites coexisted with neutral-soap (MZ) crystallites. The coexistence of two solid phases $(HZ)_1(MZ)_1$ and MZ crystallites, leads to a system with zero thermodynamic degrees of freedom [4], i.e. the concentrations of all ionic species in these solutions, and their pH, become independent of the total input carboxylate concentration, c_t. In particular, after the appearance of the second precipitate, i.e. the MZ (NaMy) crystallites, the electrolytic conductivity, κ, of the solutions becomes constant (independent of c_t) (see Fig. 1). The formation of NaMy crystallites instead of NaMy micelles means that the working temperature, 25 °C, is below the Krafft temperature for NaMy.

We measured also the electrolytic conductivity of potassium myristate (KMy) solutions. The results for three temperatures, 10, 25 and 40 °C, are shown in Fig. 2a. One sees that the κ-vs.-c_t curves have a kink at around $c_t \approx 10$ mM, and after that κ continues to increase, but with a smaller slope of the experimental dependence. Such behavior is typical for solutions in which micelles are formed above a certain surfactant concentration [17,26–28]. In particular, the kink corresponds to the critical micellization concentration (CMC). Hence, the KMy solutions (unlike the NaMy solutions) are above the Krafft temperature, even at 10 °C. In the micellar solutions of KMy, we observe also crystallites (of acid soap – see below) that coexist with the micelles.

Our goal in the present article is to investigate the coexistence of surfactant micelles and acid-soap crystallites in the solutions of KMy. This includes the determination of the amounts of myristate incorporated in micelles and in acid-soap crystallites; determination of the micelle composition and charge, and the stoichiometry of the acid soap. The effect of temperature, 40 °C vs. 25 °C, as well as the effects of added myristic acid (HZ) and inorganic electrolyte (KCl), are also examined. The development of theoretical model allows us

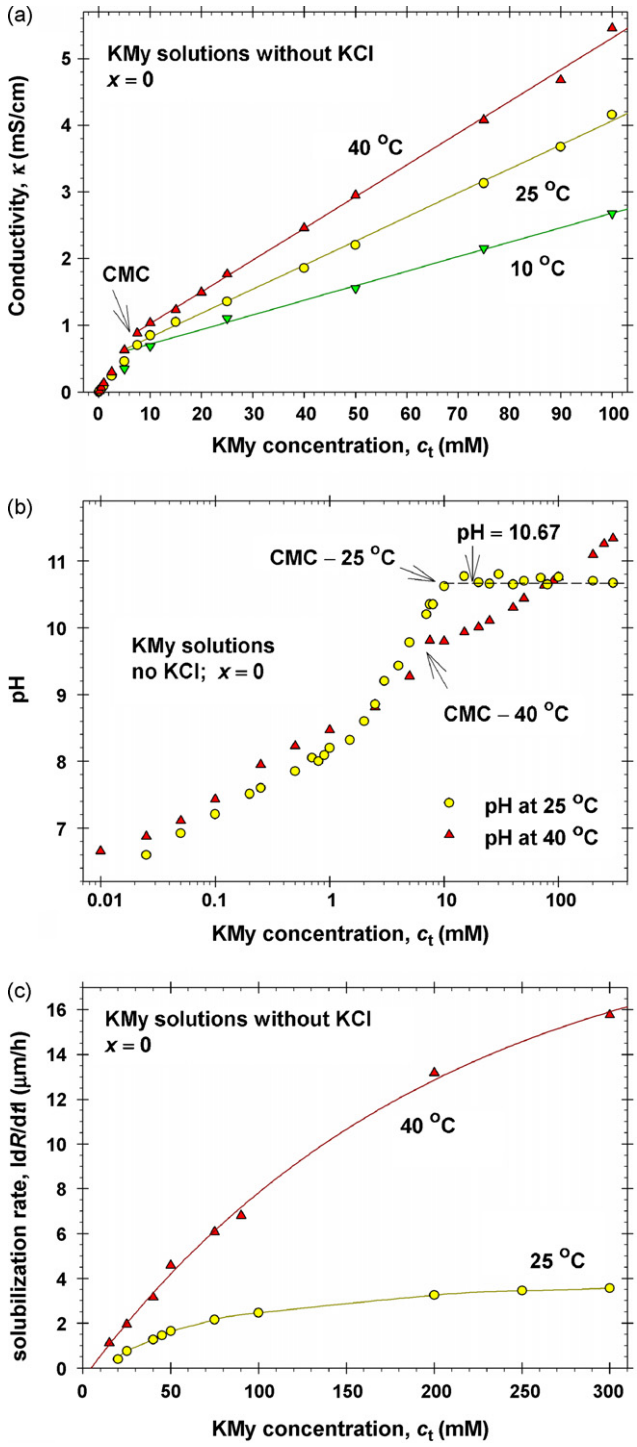

Fig. 2. Experimental results for solutions of KMy. (a) Electrolytic conductivity, κ, vs. the total carboxylate concentration, c_t, at 10, 25 and 40 °C. (b) pH vs. c_t at 25 and 40 °C. (c) Rate of solubilization of *n*-decane vs. c_t at 25 and 40 °C.

to determine the concentrations of all species in the solutions, and afterwards to interpret their surface tension isotherms.

The paper is organized as follows. In Section 2, we present the experimental materials, methods and results. In Section 3, the theory of precipitation in carboxylate soap solutions in the presence of HZ additive below the CMC is outlined. Section 4 is dedicated to the theory of carboxylate solutions with coexisting micelles and crystallites. In Section 5, theory and experiment are compared and interpretation of the data is proposed. Finally, the results and conclusions are summarized in Section 6.

2. Experimental

2.1. Materials

Solutions of potassium myristate (KMy) were prepared by using two different procedures. *Procedure 1*: KMy solutions were obtained by dissolving stoichiometric amounts of myristic acid (HMy, Fluka, 98% pure) and potassium hydroxide (KOH, Teokom, pure for analysis) at 60 °C, and stirring for 30 min. Then, the solutions were cooled down to 25 °C. *Procedure 2*: The same as Procedure 1, but commercial KMy (producer Viva Corporation) was dissolved.

In some experiments (Procedure 1), the amount of KOH was 87.5 mol% of that needed for full neutralization of HMy. The obtained solutions contain 87.5 mol% KMy and 12.5 mol% HMy. Thus, we checked the effect of added HMy on the precipitates in the investigated solutions. In other experiments, KCl (product of Sigma) was added to the solutions.

The working solutions for conductivity analysis were prepared by dissolving corresponding amounts of the collected crystallites at 60 °C to obtain a solution of a given concentration. Finally, the solutions were cooled down to the working temperature of 25 or 40 °C, and their pH and electrolytic conductivity, κ, were measured.

In a comparative series of conductivity measurements (Fig. 1), we used sodium myristate, NaMy, >99% pure (product of TCI, Tokyo, Japan). The NaMy solutions were also prepared at 60 °C by stirring for 30 min, and afterwards cooled to 25 °C.

All solutions were prepared by water that had been initially deionized (Milli Q 185 plus, Millipore, USA). Before the measurements of pH and electric conductivity, all solutions have been kept for 24 h at the working temperature to attain equilibrium between the solution and the forming crystallites.

2.2. Methods

The pH of the solutions was measured (pH-meter, Oakton Instruments, IL, USA) as a function of the total concentration of carboxylate, c_t. The temperature was kept 25 °C, except one series of measurements at 40 °C.

The electric conductivity of the solutions vs. c_t was measured by means of a conductivity-meter, Denver Instruments, USA. The temperature was 25 °C, except two series of comparative measurements at 10 and 40 °C.

The rate of solubilization was measured by means of the device described in references [29,30]. Drops of *n*-decane of initial size 30–40 μm were injected by a micropipette in a horizontal capillary loaded with the investigated solution. The radius of the diminishing drop of *n*-decane is a linear function of time, $R = R(t)$ [30]. The solubilization rate, dR/dt, is determined as a function of the input concentration of KMy.

The solutions' surface tension, σ, was measured by means of the Wilhelmy-plate method (tensiometer Krüss 10ST).

2.3. Experimental results and preliminary discussion

2.3.1. Solutions of potassium myristate (KMy)

Here and hereafter, c_t is the total input concentration of carboxylate, which includes the dissolved species (such as Z^-), the carboxylate in micellar form and in the precipitated crystallites. Fig. 2a shows experimental data for the electrolytic conductivity of KMy solutions at three temperatures: 10, 25 and 40 °C. At each temperature, the experimental curve has two linear portions with a kink at about c_t = 10 mM, which corresponds to the critical micellization concentration (CMC). The slope of the κ-vs.-c_t dependence is smaller at the greater concentrations, on the right of the kink. As mentioned above, such behavior of conductivity indicates the formation of surfactant micelles at c_t > 10 mM.

Fig. 2b shows the pH of the KMy solutions measured at 25 and 40 °C. Both curves exhibit a kink close to c_t = 10 mM. Detailed analysis and interpretation of the pH data is given in Section 5.1. Fig. 2c shows experimental results for the solubilization rate vs. c_t. The fact that solubilization is observed at c_t > 10 mM, confirms the indications from Fig. 2a and b that micelles are present in the KMy solutions for c_t > 10 mM. The increase of the solubilization rate with c_t is due to the rise of micelle concentration [30,31]. Because the micelles and the oil drops are similarly charged, they repel each other. In such case, the micelles cannot directly contact the oil drops. Instead, the mechanism of solubilization is related to the ability of the micelles to engulf oil molecules dissolved in water [29–31]. The greater solubilization rate at 40 °C (Fig. 2c) can be explained with the faster dissolution of oil from the drops at 40 °C, in comparison with 25 °C.

At T = 25 °C, the direct observations show the following. At $c_t \leq 2.5$ mM, the solutions are clear; no sedimentation of precipitates is observed. However, the microscopic observations show that fine elongated crystallites are dispersed in these solutions (Fig. 3a). At $2.5 \leq c_t \leq 40$ mM, the solutions become turbid and many small plate-like crystallites are observed. In some experiments, these crystallites could grow bigger and form sediment. At $5 \leq c_t \leq 10$ mM these crystallites look thinner and have irregular edges, whereas at $10 < c_t < 40$ mM the crystallites look thicker and have straight edges (Fig. 3b). Surprisingly, at $c_t \geq 40$ mM the solutions look clean; however, by dynamic-light-scattering (DLS) we detected a strong signal of scattered light, which is much stronger than that pro-

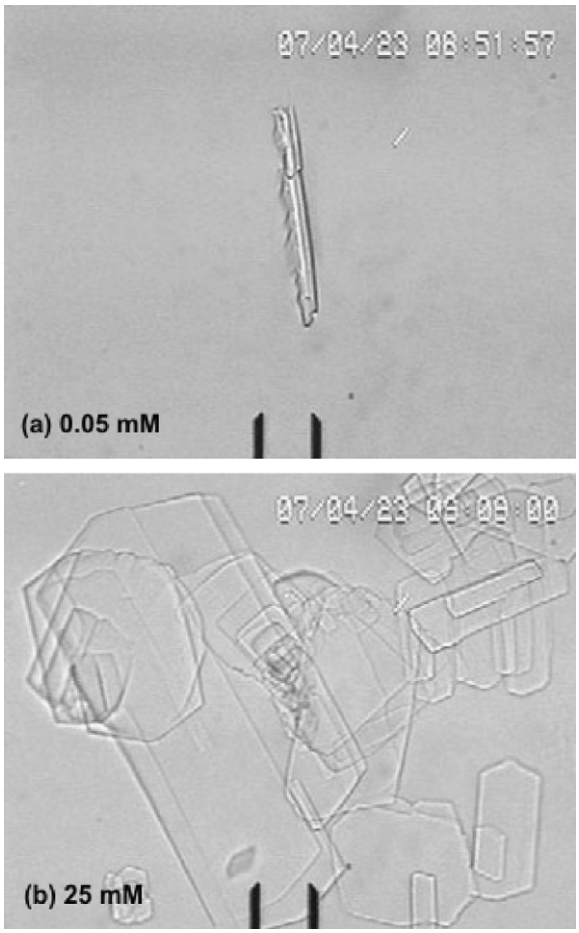

Fig. 3. Photographs of crystallites observed in solutions of KMy at two concentrations denoted in the figures; T = 25 °C; no added KCl. (a) c_t = 0.05 mM; (b) c_t = 25 mM. The reference mark is 20 μm.

duced by micellar solutions. The latter fact indicates the presence of dispersed submicrometer crystallites.

At $T = 40\,^{\circ}C$, the direct observations give similar results: At $c_t < 5$ mM, the solutions look clear, but by microscope one could observe the presence of separate small crystallites. At $5 \le c_t \le 40$ mM, the solutions are turbid and many small crystallites could be seen. At $c_t \ge 40$ mM the solutions look clean, but they strongly scatter light when investigated by DLS. Some of the latter solutions, after storage for a longer time (1 week), become turbid and micrometer-sized crystallites can be seen.

2.3.2. Solutions of 87.5 mol% KMy and 12.5 mol% HMy

In this case, c_t denotes the total carboxylate concentration, which includes 87.5 mol% KMy and 12.5 mol% HMy. The respective solutions are visibly more turbid than those without HMy (see above). Fig. 4a shows experimental data for the conductivity of KMy solutions at two concentrations of added KCl: 0 and 100 mM. Each of the two conductivity vs. c_t curves exhibits a kink, which corresponds to $c_t \approx 13$ and 5 mM, respectively, for the solutions with 0 and 100 mM KCl. Approximately, at the same values of c_t one observes kinks in the dependence of pH on c_t (see Fig. 4b). For $0.4 < c_t < 13$ mM there is a significant difference between the pH(c_t) for 0 and 100 mM KCl. At higher concentrations, both dependencies reach a plateau, which is slightly higher for the solutions with 100 mM KCl (Fig. 4b). The jump-wise change in the pH of the latter solutions at $c_t \approx 0.4$–0.5 mM can be explained with a change in the stoichiometry of the acid-soap crystallites in these solutions (see Section 5.3).

The solubilization data in Fig. 4c show that the solutions solubilize oil in the concentration regions above the kinks in Fig. 4a, which correspond to the plateaus in Fig. 4b. The latter fact indicates the presence of surfactant micelles in the aforementioned concentration regions, where we observe also crystallites. In other words, the crystallites, like these in Figs. 5b and 6b, coexist with optically invisible micelles.

In the case without added KCl, for $2 < c_t < 13$ mM, one observes the formation of elongated, knife-like crystallites (Fig. 5a). In the solubilization experiments, these crystallites attach to the surface of the oil (*n*-decane) drop, and enter inside the oil. In other words, they are hydrophobic. For $c_t > 13$ mM, the crystallites are plate-like (Fig. 5b); they neither attach to the oil–water interface, nor enter inside the oil, i.e. they are hydrophilic. The limiting concentration, $c_t = 13$ mM, corresponds to the kink in the conductivity and pH (Fig. 4a and b). This change in the shape and hydrophilicity of the crystallites can be attributed to surfactant (Z^-) adsorption on their surfaces, most probably in the form of self-assembled aggregates on the solid surface, i.e. "hemimicelles" or "admicelles".

In the case with 100 mM added KCl, the kink in both conductivity and pH are at $c_t = 5$ mM, where the solubilization also begins. Fig. 6 shows the crystallites observed in the solutions with 100 mM KCl at $c_t = 5$ and 30 mM. The stoichiometry of the acid-soap crystallites and the amounts of myristate in micellar and crystalline form are established by theoretical analysis of the data in Section 5.

3. Theory: precipitation of crystallites below the CMC

3.1. Basic equations

In this section we consider theoretical expressions for pH and conductivity of carboxylate solutions at concentrations below the onset of aggregation of the carboxylate in the form of either micelles (KMy at 25 °C) or neutral-soap crystals (NaMy at 25 °C). At these relatively low concentrations, the solutions contain no more than

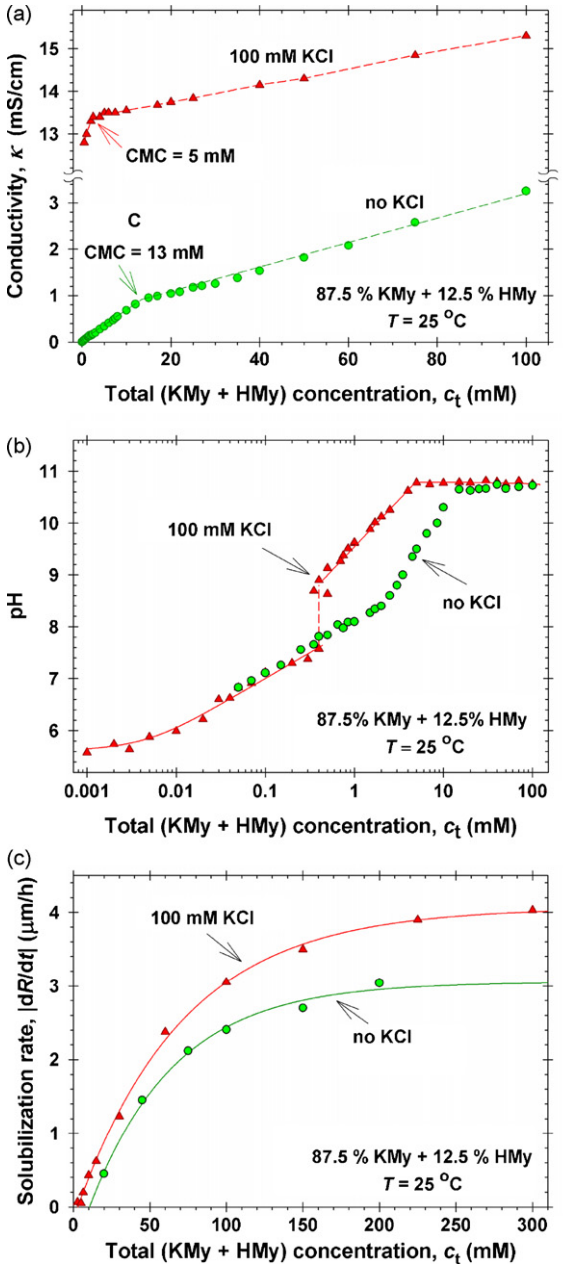

Fig. 4. Experimental results for solutions containing 87.5 mol% KMy and 12.5 mol% HMy at 0 and 100 mM added KCl and at 25 °C. (a) Electrolytic conductivity, κ, vs. the total carboxylate concentration, c_t. (b) pH vs. c_t. (c) Rate of solubilization of *n*-decane vs. c_t.

one kind of crystalline precipitates, which can be either carboxylic acid (HZ), or acid soap of certain stoichiometry *j*:*n*.

As mentioned in Section 2, in a part of our experiments we initially dissolved (at 60 °C) MZ (KMy) and HZ (HMy) at input concentrations c_{t1} and c_{t2}, respectively. After that, the solutions were cooled down to the working temperature (25 or 40 °C) and their pH was measured after 24 h equilibration at that working temperature. The total carboxylate concentration is:

$$c_t = c_{t1} + c_{t2} \tag{3.1}$$

Let us denote by $x \equiv c_{t2}/c_t$ the input molar fraction of HZ. Thus, we obtain:

$$c_{t1} = (1 - x)c_t, \quad c_{t2} = xc_t \tag{3.2}$$

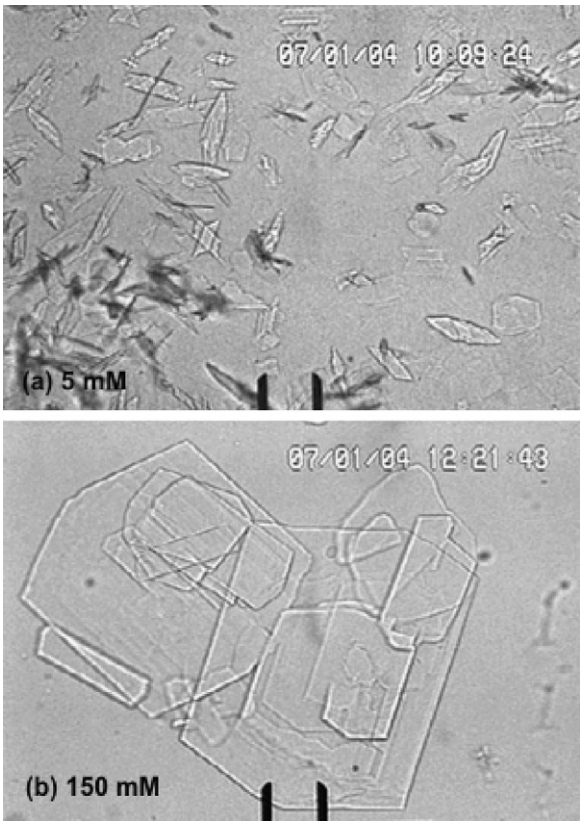

Fig. 5. Photographs of crystallites in solutions of 87.5 mol% KMy and 12.5 mol% HMy (without added KCl) at 25 °C. (a) At c_t = 5 mM, one observes sharp, knife-like crystallites that exhibit a tendency to aggregate (mark = 50 μm). (b) At c_t = 150 mM, plate-like crystallites are seen in the solutions (mark = 20 μm).

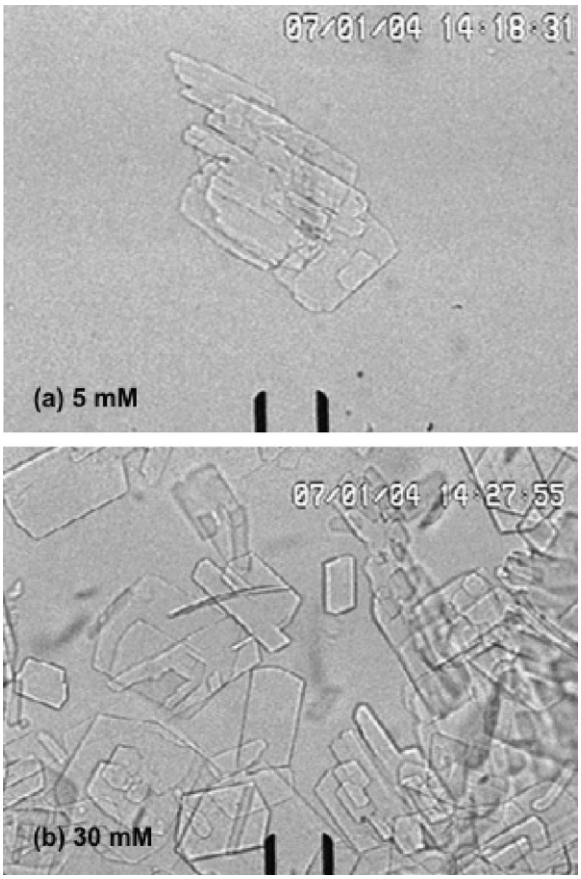

Fig. 6. Photographs of crystallites in solutions of 87.5 mol% KMy + 12.5 mol% HMy + 100 mM KCl at 25 °C. (a) c_t = 5 mM. (b) At c_t = 30 mM. The reference mark is 20 μm.

The number of molecules (per unit volume) of components M and Z that are incorporated in crystallites is:

$$m_M = (1 - x)c_t + c_A - c_M \tag{3.3}$$

$$m_Z = c_t - c_Z - c_{HZ} \tag{3.4}$$

Here, c_A is the concentration of the anions of the added inorganic electrolyte (if any). In our experiments, this was the chloride anion, Cl^-, originating from added KCl. The concentration of undissociated MZ molecules is usually small and can be neglected. In the case without micelles, the condition for electroneutrality of the solution reads:

$$c_H + c_M = c_{OH} + c_Z + c_A \tag{3.5}$$

To calculate the activity coefficient $\gamma_\pm$ at different temperatures and ionic strengths, we interpolated data from the book by Robinson and Stokes [32] for KCl solutions, and obtained the following expression:

$$\log \gamma_\pm = -\frac{0.50383\sqrt{I_T}}{1 + 1.2282\sqrt{I_T}} + 0.006920 I_T \quad \text{(for KCl)} \tag{3.6}$$

where

$$I_T \equiv \frac{T}{298.15}\frac{I}{\rho_w(T)}; \tag{3.7}$$

Here, I is the solution's ionic strength (mol/L); T is the absolute temperature (°K); $\rho_w(T)$ is the mass density of water (kg/L) at the respective temperature; I_T is an effective ionic strength (mol/kg). Eq. (3.6) predicts log $\gamma_\pm$ with relative error smaller than 0.15% in the temperature interval from 15 to 45 °C.

Likewise, we obtained an analogue of Eq. (3.6) for NaCl solutions:

$$\log \gamma_\pm = -\frac{0.50911\sqrt{I_T}}{1 + 1.3754\sqrt{I_T}} + 0.031706 I_T \quad \text{(for NaCl)} \tag{3.8}$$

where I_T is given by Eq. (3.7). Eq. (3.8) predicts log $\gamma_\pm$ with a relative error lower than 0.25% in the temperature range from 15 to 45 °C.

The dissociation equilibrium of the carboxylic acid molecules is described by the equation:

$$c_H c_Z \gamma_\pm^2 = K_A c_{HZ} \tag{3.9}$$

where $K_A = 1.25 \times 10^{-5}$ is the equilibrium constant of the reaction $H^+ + Z^- \leftrightarrow HZ$ [4]. Here and hereafter, the concentrations in the equilibrium constants are expressed in molarity (M). Likewise, for the dissociation equilibrium of water we have:

$$c_H c_{OH} \gamma_\pm^2 = K_W = 6.81 \times 10^{-15} (\text{at } 20\,^\circ\text{C}) \tag{3.10}$$

The carboxylic acid is soluble in water for $c_{HZ} < S_{HZ}$, where S_{HZ} is its equilibrium solubility. Based on experimental data, Lucassen [4] obtained the following expression for the solubility of a fatty acid containing n carbon atoms:

$$\log S_{HZ} = -0.65n + 2.82 \tag{3.11}$$

For myristic acid (n = 14), Eq. (3.11) yields $S_{HZ} = 5.25 \times 10^{-7}$ M. Analogously, the solubility product K_{11} of the 1:1 potassium acid soap is [4]:

$$\frac{1}{2}\log K_{11} = -0.65n + 0.70 \tag{3.12}$$

The solubility product, K_{MZ}, of potassium neutral soaps is [4]:

$$\log K_{MZ} = -0.65n + 5.41 \tag{3.13}$$

Furthermore, knowing the values of S_{HZ}, K_{11} and K_{MZ}, we can estimate the solubility product, K_{jn}, of a j:n acid-soap complex, $(HZ)_j(MZ)_n$, with the help of the expressions [17]:

$$\log K_{jn} = j\log\left(\frac{jK_{11}}{n}\right) + (n-j)\log\left[\frac{(n-j)K_{MZ}}{n}\right] \quad \text{for } n > j \tag{3.14}$$

$$\log K_{jn} = n\log\left(\frac{nK_{11}}{j}\right) + (j-n)\log\left[\frac{(j-n)K_{HZ}}{j}\right] \quad \text{for } n < j \tag{3.15}$$

where $K_{HZ} \equiv K_A S_{HZ}$ is the solubility product of the carboxylic acid. These equilibrium constants will be used below for the quantitative interpretation of the data.

In a preceding paper [17], the theory of precipitation in carboxylate soap solutions was presented for the case without added carboxylic acid (HZ), i.e. for $x = 0$. Below, we will give a generalization of the equations for the case where there is added carboxylic acid, i.e. $x > 0$.

3.2. Solutions with precipitate of carboxylic acid (HZ)

In this case, the concentration of the carboxylic acid is fixed:

$$c_{HZ} = S_{HZ} = \text{constant} \tag{3.16}$$

From Eqs. (3.9) and (3.16), we express the concentration of the carboxylate ion:

$$c_Z = \frac{K_{HZ}}{\gamma_\pm^2 c_H} \quad (K_{HZ} \equiv K_A S_{HZ}) \tag{3.17}$$

Because the precipitate is of HZ alone, metal counterions, M^+, are not incorporated in precipitates and then $m_M = 0$. Then, Eq. (3.3) reduces to:

$$c_M = (1-x)c_t + c_A \tag{3.18}$$

With the help of Eqs. (3.10), (3.17) and (3.18) we bring the electroneutrality condition, Eq. (3.5), in the form:

$$[c_H + (1-x)c_t]c_H\gamma_\pm^2 = K_t, \tag{3.19}$$

where $K_t \equiv K_{HZ} + K_W$. For myristic acid $K_W \ll K_{HZ}$, which means that $K_t \approx K_{HZ}$. Eq. (3.19) represents a quadratic equation for calculation of c_H at a given c_t. It determines the dependence $pH(c_t)$ for the case of HZ precipitate. On the basis of Eq. (3.19), two mutually complementary approaches have been proposed in the literature for identification of HZ precipitate:

(a) *Linearization method* by Lucassen [4]: If c_H in the brackets in Eq. (3.19) is negligible in comparison with $(1-x)c_t$, and in addition, $\gamma_\pm \approx 1$, by taking logarithm we obtain:

$$\text{pH} = \log c_t - \log\left[\frac{K_t}{(1-x)}\right] \tag{3.20}$$

Eq. (3.20) indicates that if the precipitate is of HZ, then the data for pH vs. $\log c_t$, should lie on a straight line of slope = +1.

(b) *Method of characteristic functions* [17]: Having in mind that $\text{pH} = -\log(c_H\gamma_\pm)$, by taking logarithm of Eq. (3.19) we obtain:

$$f_{HZ} \equiv \log[c_H\gamma_\pm + (1-x)c_t\gamma_\pm] - \text{pH} = \log K_t \tag{3.21}$$

By definition, f_{HZ} is the *characteristic function* for precipitate of carboxylic acid (HZ). Note that f_{HZ} depends only on the concentrations c_H and c_t, which are known from the experiment. In particular, the experiment yields $c_H(c_t)$ (see e.g. Figs. 2b and 4b). Then, if we plot f_{HZ} vs. c_t, we will have $f_{HZ} = \text{const.} = \log K_t$ in the region where HZ precipitate is present. Thus, from the plot of the function $f_{HZ}(c_t)$ we simultaneously determine the concentration region with HZ precipitate and the value of the constant $\log K_t \approx \log K_{HZ}$.

3.3. Solutions with precipitate of acid soap, $(HZ)_j(MZ)_n$

The subtraction of Eq. (3.3) from Eq. (3.4) yields:

$$m_Z - m_M = xc_t - c_A + c_M - c_Z - c_{HZ} \tag{3.22}$$

In Eq. (3.22), we substitute c_M from the electroneutrality condition, Eq. (3.5):

$$m_Z - m_M = c_{OH} + xc_t - c_H - c_{HZ} \tag{3.23}$$

If a precipitate of $(HZ)_j(MZ)_n$ acid soap is present, we have:

$$\frac{m_M}{m_Z} = \omega \quad \text{where } \omega \equiv \frac{n}{j+n} \tag{3.24}$$

Then, Eq. (3.23) acquires the form:

$$(1-\omega)m_Z = c_{OH} + xc_t - c_H - c_{HZ} \tag{3.25}$$

c_{HZ} cannot be greater than the equilibrium solubility of the carboxylic acid S_{HZ} (which is very low), and in the region of acid-soaps precipitates we have $c_H \ll c_{OH}$. Then, Eq. (3.25) can be simplified:

$$m_Z \approx \frac{1}{1-\omega}(xc_t + c_{OH}) \tag{3.26}$$

One sees that the amount of acid-soap precipitate grows with the rise of x. Further, substituting Eqs. (3.24) and (3.26) into Eqs. (3.3) and (3.4), we derive:

$$c_Z \approx \xi c_t - \frac{1}{1-\omega}c_{OH} \tag{3.27}$$

$$c_M \approx \xi c_t + c_A - \frac{\omega}{1-\omega}c_{OH} \tag{3.28}$$

where

$$\xi \equiv 1 - \frac{x}{1-\omega} \tag{3.29}$$

The solution's ionic strength is:

$$I = c_M + c_H \approx c_M \approx \xi c_t + c_A - \frac{\omega}{1-\omega}c_{OH} \tag{3.30}$$

where we have used Eq. (3.28) and the fact that $c_H \ll c_M$ at our experimental conditions. Under the same conditions, the last c_{OH}-terms in Eqs. (3.27) and (3.28) are also small, so these equations can be further simplified:

$$c_Z \approx \xi c_t \quad \text{and} \quad c_M \approx \xi c_t + c_A \tag{3.31}$$

The solubility product for a j:n acid soap is:

$$c_H^j c_M^n c_Z^{j+n}\gamma_\pm^{2j+2n} = K_{jn} \qquad (j, n = 1, 2, 3, \ldots) \tag{3.32}$$

where K_{jn} is equilibrium constant (see Eqs. (3.14)–(3.15)). The two methods for identification of a j:n acid-soap precipitate are as follows.

(a) *Linearization method* [4,17]: If $c_A = 0$ and $\gamma_\pm \approx 1$, by taking logarithm of Eq. (3.32) and using Eq. (3.31), we obtain:

$$\text{pH} \approx \left(1 + \frac{2n}{j}\right)\log c_t - \left(\frac{1}{j}\right)\log\left(\frac{K_{jn}}{\xi^{j+2n}}\right) \tag{3.33}$$

Eq. (3.33) indicates that if the precipitate is of j:n acid soap, then the data for pH, plotted vs. $\log c_t$, must lie on a straight line of slope = $1 + 2n/j$. Thus, from the slope of the line we could determine n/j, i.e. the stoichiometry of the acid soap. This method is

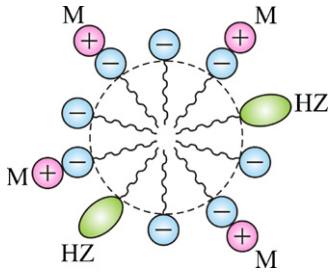

Fig. 7. Sketch of a mixed carboxylate micelle, which is composed of carboxylate anions, Z^-, bound counterions, M^+, and undissociated fatty acid molecules, HZ (in Section 4.3, we arrive at the conclusion that the micelles do not contain HZ).

not so accurate because of the used approximations. It is appropriate for an initial estimate of the ratio j:n. The more accurate method is as follows:

(b) *Method of characteristic functions* [17]: In view of Eq. (3.31), by taking logarithm of Eq. (3.32), we obtain:

$$f_{jn} \equiv \log[(\xi c_t)^{j+n}(\xi c_t + c_A)^n \gamma_\pm^{j+2n}] - j \quad \mathrm{pH} = \log K_{jn} \tag{3.34}$$

By definition, f_{jn} is the *characteristic function* for precipitate of $(HZ)_j(MZ)_n$ acid soap. The procedure for calculating $f_{jn}(c_t)$ is the following:

1. The input quantities are c_t, c_A, x, and the experimental dependence $pH(c_t)$.
2. With tentative values of j and n, we calculate ξ using Eqs. (3.24) and (3.29).
3. From Eq. (3.30), we determine the ionic strength, I; afterwards, from Eqs. (3.6)–(3.7) we find $\gamma_\pm$.
4. We calculate $f_{jn}(c_t)$ by means of its definition in Eq. (3.34).

If there is really a precipitate of acid soap with the presumed stoichiometry, j:n, then the plot of f_{jn} vs. c_t will have a plateau, $f_{jn} = \mathrm{const.} = \log K_{in}$, in the region of c_t values where such precipitate exists. Thus, from the graph of $f_{jn}(c_t)$ we simultaneously determine the value of $\log K_{jn}$ and the concentration region with $(HZ)_j(MZ)_n$ precipitate.

If there is no plateau of $f_{jn}(c_t)$ for the assumed stoichiometry j:n, then we try with other values of j and n, until we find a characteristic function which has a plateau. A good initial approximation for j:n can be obtained by means of the linearization method, see above.

For $x = 0$ (and $\xi = 1$) all equations in the present Section 3 reduce to the respective equations in reference [17].

4. Coexistence of micelles and acid-soap crystallites

4.1. Chemical equilibrium between micelles and solution

In general, the micelles in the investigated solutions could contain carboxylate anions, Z^-, bound counterions, M^+, and undissociated carboxylic-acid molecules, HZ (see Fig. 7). Formally, the micellization can be considered as a chemical reaction: $Z^- + M^+ + H^+ \leftrightarrow$ micelle. At equilibrium, the relationship between the chemical potentials of these species is:

$$n_Z\mu_Z + n_M\mu_M + n_H\mu_H = \mu_{mic} \tag{4.1}$$

where n_X (X = Z, M, H) is the average number of molecules of component X in a micelle; μ_X is their chemical potential, and the chemical potential of the micelle is μ_{mic}. At equilibrium, the chemical potential of each ion incorporated in micelles is equal to the chemical potential of the same ion in the bulk of solution:

$$\mu_X = \mu_X^{(0,l)} + kT\ln(c_X\gamma_\pm), \quad (X = \mathrm{Z, M, H}) \tag{4.2}$$

where k is the Boltzmann constant, T is the absolute temperature, $\mu_X^{(0,l)}$ and c_X are the standard chemical potentials and concentrations of the respective ions in the aqueous phase and, as usual, $\gamma_\pm$ is the activity coefficient. The analogous expression for the micelles reads:

$$\mu_{mic} = \mu_{mic}^{(0,l)} + kT\ln a_{mic} \tag{4.3}$$

where a_{mic} and $\mu_{mic}^{(0,l)}$ are the micelle activity and standard chemical potential. The substitution of Eqs. (4.2)–(4.3) into Eq. (4.1), yields:

$$\ln(c_Z\gamma_\pm) + \frac{n_M}{n_Z}\ln(c_M\gamma_\pm) + \frac{n_H}{n_Z}\ln(c_H\gamma_\pm) = \frac{\Delta\mu_{mic}}{kT} + \frac{1}{n_Z}\ln a_{mic} \tag{4.4}$$

where

$$\Delta\mu_{mic} \equiv \frac{1}{n_Z}\mu_{mic}^{(0,l)} - \mu_Z^{(0,l)} - \frac{n_M}{n_Z}\mu_M^{(0,l)} - \frac{n_H}{n_Z}\mu_H^{(0,l)} \tag{4.5}$$

Note that $n_Z \equiv N_{agg}$ is the micelle aggregation number. Usually, $N_{agg} \geq 60$ and the last term in Eq. (4.4) can be neglected. Thus, the condition for chemical equilibrium between the micelles and solution acquires the form:

$$(c_Z\gamma_\pm)(c_M\gamma_\pm)^\theta(c_H\gamma_\pm)^\eta = K_{mic} \tag{4.6}$$

where

$$\theta \equiv \frac{n_M}{n_Z}, \quad \eta \equiv \frac{n_H}{n_Z}, \quad K_{mic} \equiv \exp\left(\frac{\Delta\mu_{mic}}{kT}\right) \tag{4.7}$$

In the special case $\eta = 0$ and $\gamma_\pm \approx 1$, from Eq. (4.6) we derive:

$$\log c_Z = \log K_{mic} - \theta\log c_M \tag{4.8}$$

This is a known relationship for ionic surfactants: $\log(\mathrm{CMC}) \equiv \log(c_Z)$ decreases linearly with the log of the bulk concentration of counterions, c_M [4,33,34]. The experimentally observed linear dependencies for various ionic surfactants confirm that K_{mic} and θ can be really treated as constants [4,33,34].

4.2. Balances of masses and electric charges

Here and hereafter, $m_Y^{(as)}$ and $m_Y^{(mic)}$ denote the number of atoms of component Y (Y = M, Z) incorporated, respectively, in acid-soap crystallites and micelles, per unit volume. In view of Eqs. (4.7) and (3.24), we have:

$$\frac{m_M^{(mic)}}{m_Z^{(mic)}} = \theta, \quad \frac{m_M^{(as)}}{m_Z^{(as)}} = \omega = \frac{n}{j+n} \tag{4.9}$$

The latter relation holds for $(HZ)_j(MZ)_n$ acid-soap precipitate. As limiting cases, we have $\omega = 0$ (HZ precipitate) and $\omega = 1$ (MZ precipitate). Thus, in general $0 \leq \omega \leq 1$. Eq. (3.4) can be represented in the form:

$$m_Z \equiv m_Z^{(mic)} + m_Z^{(as)} = c_t - c_Z - c_{HZ} \tag{4.10}$$

Likewise, $m_M \equiv m_M^{(mic)} + m_M^{(as)}$, and then in view of Eq. (4.9), we can bring Eq. (3.3) in the form:

$$\theta m_Z^{(mic)} + \omega m_Z^{(as)} = (1-x)c_t + c_A - c_M \tag{4.11}$$

Eqs. (4.10) and (4.11) represent a linear system for $m_Z^{(mic)}$ and $m_Z^{(as)}$, whose solution is:

$$(\theta-\omega)\,m_Z^{(mic)} = (1-x-\omega)c_t + c_A - c_M + \omega c_Z + \omega c_{HZ} \tag{4.12}$$

$$(\theta-\omega)\,m_Z^{(as)} = -(1-x-\theta)c_t - c_A + c_M - \theta c_Z - \theta c_{HZ} \tag{4.13}$$

In the presence of micelles, the electroneutrality condition reads:

$$c_M + c_H = c_Z + c_A + c_{OH} + (1-\theta-\eta)m_Z^{(mic)} \tag{4.14}$$

where the last term accounts for the electric charge of the micelles. Subtracting Eq. (4.14) from Eq. (4.12), we derive:

$$m_Z^{(mic)} = \frac{1}{1-\omega-\eta}[(1-\omega-x)c_t - (1-\omega)c_Z + \omega c_{HZ} + c_H - c_{OH}] \quad (4.15)$$

Further, substituting Eq. (4.15) into Eq. (4.10), we obtain:

$$m_Z^{(as)} = \frac{1}{1-\omega-\eta}[(x-\eta)c_t + \eta c_Z - (1-\eta)c_{HZ} - c_H + c_{OH}] \quad (4.16)$$

At our experimental conditions, the concentrations c_H and c_{HZ} are small and can be neglected in Eqs. (4.15) and (4.16), which acquire the following simpler form:

$$m_Z^{(mic)} = \frac{1}{1-\omega-\eta}[(1-\omega)(\xi c_t - c_Z) - c_{OH}] \quad (4.17)$$

$$m_Z^{(as)} = \frac{1}{1-\omega-\eta}[c_{OH} + (x-\eta)c_t + \eta c_Z] \quad (4.18)$$

where ξ is defined by Eq. (3.29).

4.3. Discussion on the issue of micelle composition

At concentrations much greater than CMC, we have $c_t \gg c_Z$, where as usual, c_t is the total input carboxylate concentration and c_Z is the concentration of the Z^- monomers. In addition, if there is no added HZ, we have $x = 0$ and $\xi = 1$. Then, Eqs. (4.17) and (4.18) reduce to:

$$m_Z^{(mic)} \approx \frac{1}{1-\omega-\eta}[(1-\omega)c_t - c_{OH}] \quad (4.19)$$

$$m_Z^{(as)} \approx \frac{1}{1-\omega-\eta}(c_{OH} - \eta c_t) \quad (4.20)$$

The acceleration of solubilization with the increase of carboxylate concentration (Figs. 2c and 4c) indicate that $m_Z^{(mic)}$ increases with rise of c_t. Then, from Eq. (4.19) it follows:

$$1-\omega-\eta > 0 \quad (4.21)$$

Consequently, for $\eta > 0$ the coefficient before c_t in Eq. (4.19) is

$$\frac{1-\omega}{1-\omega-\eta} = 1 + \frac{\eta}{1-\omega-\eta} > 1 \quad (4.22)$$

If the last term in Eq. (4.19), that with c_{OH}, is small (which is the usual situation), Eq. (4.22) yields $m_Z^{(mic)} > c_t$, i.e. the amount of carboxylate molecules incorporated in micelles is greater that the total input amount of carboxylate molecules, which is a nonsense. Logically, there are two ways to avoid this problem:

(1) To assume that the two terms in the brackets in Eqs. (4.19) are comparable by magnitude for the whole investigated range of c_t values;
(2) To assume that $\eta = 0$, i.e. that the micelles do not contain HZ molecules.

The first hypothesis presumes a strong relationship between the concentration of micelles and the solution's pH. This seems physically unrealistic, because the formation of micelles by the ionic surfactants is a general phenomenon, the variation of pH being a side effect in the case of carboxylates.

For this reason, we accept the second hypothesis, $\eta = 0$, i.e. the micelles do not contain HZ molecules. The latter are contained only in the acid soap that coexists with the micelles. In other words, the presence of HZ leads to "solidification" of the formed aggregates, which represent crystallites of acid soap, whereas the formed micelles ("soft matter") are composed only of Z^- and M^+. If $\eta = 0$, then Eqs. (4.17) and (4.18) reduce to:

$$m_Z^{(mic)} = \xi c_t - c_Z - \frac{c_{OH}}{1-\omega} \quad (4.23)$$

$$m_Z^{(as)} = \frac{1}{1-\omega}(c_{OH} + x c_t) \quad (4.24)$$

4.4. Expressions for the ionic strength and pH

Substituting Eq. (4.24) into Eq. (4.13), we obtain:

$$c_M \approx c_A + (1-\theta)\xi c_t + \theta c_Z + \frac{\theta-\omega}{1-\omega}c_{OH} \quad (4.25)$$

The ionic strength is used only for calculation of the activity coefficient $\gamma_\pm$, and therefore, the following leading order approximation can be used:

$$I \approx \frac{1}{2}(c_M + c_A + c_Z) \approx c_A + \frac{1}{2}[(1-\theta)\xi c_t + (1+\theta)c_Z] \quad (4.26)$$

At the last step we have used Eq. (4.25), where the c_{OH}-term has been neglected. For the sake of applications, it is convenient to represent Eq. (4.6) (with $\eta = 0$) and Eq. (3.32) in the form:

$$\log(c_Z\gamma_\pm) + \theta \log(c_M\gamma_\pm) = \log K_{mic} \quad (4.27)$$

$$\log(c_Z\gamma_\pm) + \omega \log(c_M\gamma_\pm) = \frac{1}{j+n}\log K_{jn} + (1-\omega)\mathrm{pH} \quad (4.28)$$

Subtracting Eq. (4.27) from Eq. (4.28), we derive:

$$\mathrm{pH} = \frac{\omega-\theta}{1-\omega}\log(c_M\gamma_\pm) + \frac{1}{1-\omega}\left(\log K_{mic} - \frac{\log K_{jn}}{j+n}\right) \quad (4.29)$$

Eq. (4.29) can be used for interpretation of the pH data in the presence of micelles. For this goal, pH is plotted vs. $\log(c_M\gamma_\pm)$ where, at concentrations much above the CMC, c_M can be calculated from a simplified version of Eq. (4.25):

$$c_M \approx c_A + (1-\theta)\xi c_t \quad (4.30)$$

Eqs. (4.29) and (4.30) show that in the presence of micelles three cases are possible. First, at $\omega = \theta$ the pH is *independent* of the total carboxylate concentration, c_t. Second, for $\omega < \theta$ the pH *decreases* with the rise of c_t; such a situation has been discussed by Lucassen [4]. Third, for $\omega > \theta$ the pH increases with the rise of c_t, which is the case of micellar KMy solutions at 40 °C (see Section 5.1). In our experiments with KMy solutions under different conditions, all the three aforementioned cases have been observed (see below).

4.5. Expressions for the electrolytic conductivity κ

The conductivity of the investigated solutions can be expressed in the form [35,36]:

$$\kappa = \sum_i \lambda_i^0 c_i - AI^{3/2} + BI^2 \quad (4.31)$$

where the summation is carried out over all ionic species, whose concentrations are denoted c_i; λ_i^0 are the respective molar ionic conductances at infinite dilution; as usual, I is the ionic strength; A and B are the empirical coefficients of the augmented Kohlrausch law [37], which account for the interactions between the ions and have been tabulated for various electrolytes [38]. The coefficients A and B are practically the same for different 1:1 electrolytes [35,36].

For a micellar solution of carboxylate, MZ, with added inorganic electrolyte, MA, we have:

$$\sum_i \lambda_i^0 c_i = \lambda_M^0 c_M + \lambda_Z^0 c_Z + \lambda_A^0 c_A + \lambda_{OH}^0 c_{OH} + \lambda_H^0 c_H + \lambda_{mic} c_{mic} \quad (4.32)$$

Table 1
Molar conductances, λ_i^0 (cm^2 S/mol), of several ions in aqueous solutions and Kohlrausch coefficients, A ($mS\,cm^{-1}\,M^{-3/2}$) and B ($mS\,cm^{-1}\,M^{-2}$), at two different temperatures.

Parameter[a]	25 °C	40 °C
λ_K^0	73.50	95.69
λ_{Na}^0	50.10	67.56
λ_{Cl}^0	76.35	100.6
λ_{OH}^0	198.3	260.6
λ_{My}^0	20.44	27.9
$\tilde{\lambda}_{mic}$	3.82	5.21
A	95.20	204.4
B	92.72	–

[a] The values of λ_K^0, λ_{Na}^0, λ_{Cl}^0 and λ_{OH}^0 are from handbooks [35,38,40]; the values of λ_{My}^0, A and B are from reference [36], and the values of $\tilde{\lambda}_{mic}$ are from Eq. (4.35).

where c_{mic}, and λ_{mic} are the concentration and conductance of the micelles. Further, we will use the relationships:

$$c_{mic} = \frac{m_Z^{(mic)}}{N_{agg}} \quad \text{and} \quad \lambda_{mic} \equiv (1-\theta)N_{agg}\tilde{\lambda}_{mic} \tag{4.33}$$

where the latter relationship represents a definition of $\tilde{\lambda}_{mic}$; $(1-\theta)N_{agg}$ is the number of elementary electric charges per micelle. Then, the last term in Eq. (4.32) acquires the form:

$$\lambda_{mic}c_{mic} = (1-\theta)\tilde{\lambda}_{mic}m_Z^{(mic)} \tag{4.34}$$

$\tilde{\lambda}_{mic}$ can be estimated from the expression [35]:

$$\tilde{\lambda}_{mic} = \frac{e^2 N_A}{6\pi\eta_w r_{mic}} \tag{4.35}$$

where N_A is the Avogadro number, η_w is the viscosity of water, r_{mic} is the micelle radius, and e is the elementary electric charge. Because the micelle radius is approximately equal to the length of the surfactant molecule, using molecular-size considerations [39], from Eq. (4.35) we estimate $\tilde{\lambda}_{mic} = 3.82\ cm^2$ S/mol for KMy at 25 °C ($\eta_w = 0.8903$ mPa s). $\tilde{\lambda}_{mic}$ is relatively small as compared to the conductance of the small ions, like K^+ (see Table 1). In other words, the main contribution of the micelles to conductivity comes from the counterions dissociated from their ionizable groups. It should be noted that all conductances depend on temperature, because $\lambda_i^0 \propto 1/\eta_w$ and the viscosity η_w essentially depends on T.

Finally, we combine Eqs. (4.31), (4.32) and (4.34), and substitute $m_Z^{(mic)}$ from Eq. (4.23) and c_M from Eq. (4.25). The resulting expression for the electrolytic conductivity of micellar carboxylate solutions reads:

$$\kappa \approx (\lambda_M^0 + \tilde{\lambda}_{mic})(1-\theta)\xi c_t + [\lambda_Z^0 + \lambda_M^0\theta - \tilde{\lambda}_{mic}(1-\theta)]c_Z + (\lambda_A^0 + \lambda_M^0)c_A + \left(\lambda_{OH}^0 + \lambda_M^0\frac{\theta-\omega}{1-\omega} - \tilde{\lambda}_{mic}\frac{1-\theta}{1-\omega}\right)c_{OH} - AI^{3/2} + BI^2 \tag{4.36}$$

We have neglected the contribution of c_H, which is negligible for the pH values in our experiments. The values of the other parameters in Eq. (4.36) are given in Table 1 for the two working temperatures, 25 and 40 °C.

4.6. Principles of the procedure for data processing

We simultaneously processed our experimental data for pH-vs.-c_t and for the conductivity, κ-vs.-c_t. For micellar solutions that coexist with carboxylate crystallites, the used procedure is as follows:

1. The input information consists of the experimental points of the dependences pH-vs.-c_t and κ-vs.-c_t, like those in Fig. 2a and b, including the values of c_t at the CMC, $c_{t,cmc}$, determined from the kink in the respective experimental dependence. The input fraction, x, of HZ in the total amount of carboxylate, and the concentration, c_A, of added inorganic electrolyte are also input parameters.
2. We choose tentative values of the degree of counterion binding to the micelles, θ, and of the parameters j and n that characterize the stoichiometry of the j:n acid soap. Then $\omega = n/(j+n)$; $\xi = 1 - x/(1-\omega)$, and the solubility product of the acid soap, K_{jn}, is estimated from Eqs. (3.14)–(3.15). Because the latter equations are approximate, in most cases we used ω and K_{jn} as adjustable parameters, instead of j and n.
3. At $c_t = c_{t,cmc}$, we calculate c_Z and c_M from Eq. (3.31):

$$c_Z \approx \xi c_{t,cmc} \quad \text{and} \quad c_M \approx \xi c_{t,cmc} + c_A \tag{4.37}$$

The respective value of the ionic strength, $I \approx c_M$, is substituted in Eqs. (3.6)–(3.7) and the value of the activity coefficient, $\gamma_\pm$, in CMC is computed. Next, the micellization constant, K_{mic}, is calculated from Eq. (4.27).

4. For a given c_t above the CMC, we choose a tentative value of c_Z. Then, we calculate c_M from Eq. (4.25) (with neglected c_{OH}-term); I from Eq. (4.26) and $\gamma_\pm$ from Eqs. (3.6)–(3.7). The results are substituted in Eq. (4.27), which is considered as an implicit equation for determining c_Z that is solved numerically by the bisection method. Thus, for each given c_t we determine c_Z, c_M, I, and $\gamma_\pm$.
5. For the given c_t and $\omega < 1$, the theoretical value of pH is calculated from Eq. (4.28). After that, using Eq. (3.10) we estimate c_{OH}:

$$c_{OH} = \frac{6.81}{\gamma_\pm}10^{pH-15} \tag{4.38}$$

6. The theoretical value of the solution's conductivity, κ, is calculated from Eq. (4.36).
7. To fit simultaneously the data for pH-vs.-c_t and κ-vs.-c_t, we calculate the merit functions:

$$\chi_{pH}^2(\theta,\omega,K_{jn}) = \sum_{i=1}^{N_{pH}}\left[\frac{pH^{(i)} - pH(c_t^{(i)},\theta,\omega,K_{jn})}{\sigma_{pH,exp}}\right]^2 \tag{4.39}$$

$$\chi_\kappa^2(\theta,\omega,K_{jn}) = \sum_{i=1}^{N_\kappa}\left[\frac{\kappa^{(i)} - \kappa(c_t^{(i)},\theta,\omega,K_{jn})}{\sigma_{\kappa,exp}}\right]^2 \tag{4.40}$$

Here, the superscript "(i)" numbers the experimental points; N_{pH} and N_κ are the total numbers of points for pH and κ, respectively; $pH(c_t^{(i)},\theta,\omega,K_{jn})$ and $\kappa(c_t^{(i)},\theta,\omega,K_{jn})$ are theoretical values of pH and κ, calculated at steps 5 and 6 above. For each experimental point, several measurements of pH and κ have been carried out. $\sigma_{pH,exp}$ and $\sigma_{\kappa,exp}$ are estimates for the standard deviations of the respective data, obtained by averaging over all experimental points.

8. We numerically minimize the sum $\chi_\kappa^2 + \chi_{pH}^2$ and determine the values of θ, ω, and K_{jn} that correspond to the best fit. The scaling with $\sigma_{pH,exp}$ and $\sigma_{\kappa,exp}$ in the right-hand sides of Eqs. (4.39) and (4.40) makes χ_κ^2 and χ_{pH}^2 comparable by magnitude and gives equal weight of the two sets of data (for pH and κ) in the minimization.
9. The amounts of carboxylate molecules that are incorporated in micelles and acid-soap precipitates per unit volume, $m_Z^{(mic)}$ and $m_Z^{(as)}$, are calculated from Eqs. (4.23) and (4.24).

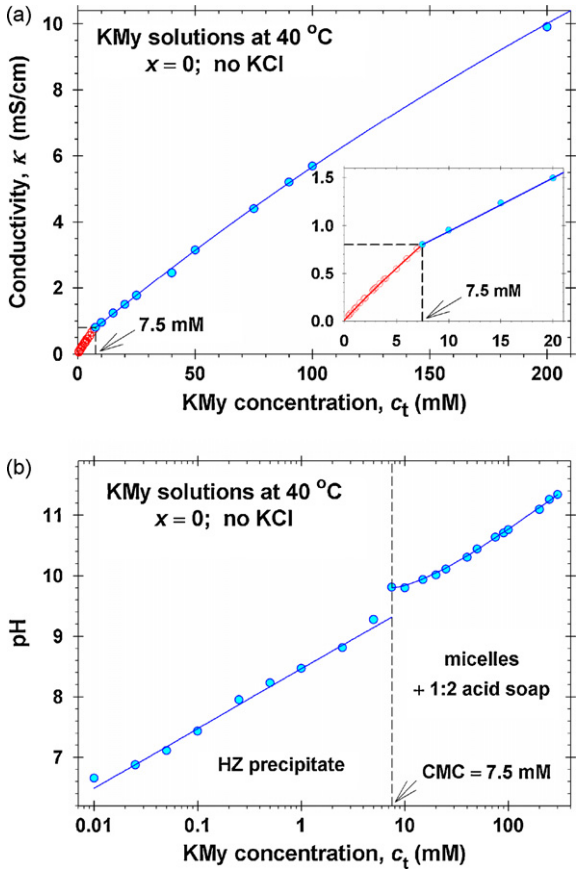

Fig. 8. (a) Electrolytic conductivity, κ, and (b) pH of KMy solutions at 40 °C. The data indicate that CMC ≈ 7.5 mM. For c_t < 7.5 mM HZ precipitate is present, whereas for c_t > 7.5 mM the solutions contain 1:2 acid soap and micelles.

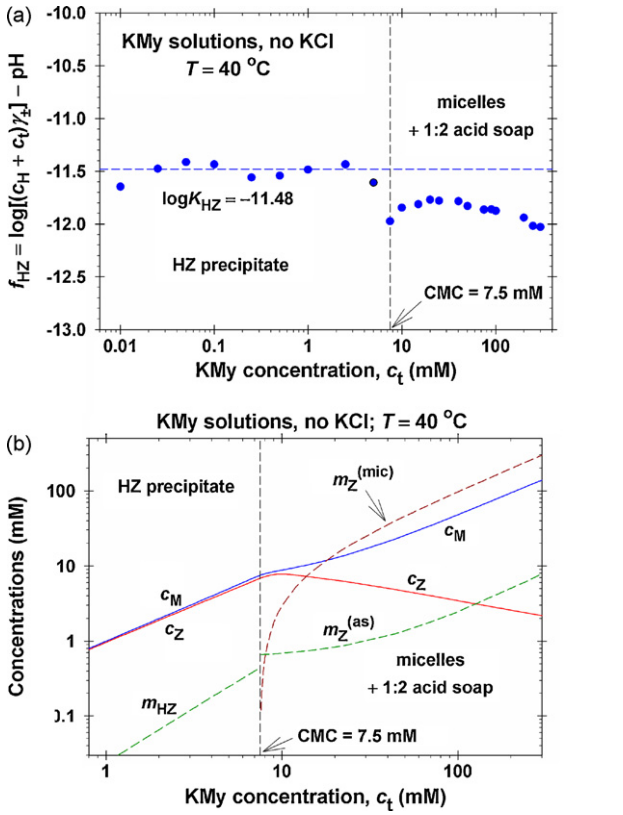

Fig. 9. Results for KMy at 40 °C (no added HZ or KCl). (a) Precipitation diagram: the plateau of $f_{HZ}(c_t)$ shows the region in which HZ precipitate is present, and the level of the plateau gives K_{HZ}. (b) Calculated concentrations of the various species in the KMy solutions; the concentrations of precipitates, m_{HZ} and $m_Z^{(as)}$, correspond to uniform dispersion of the crystallites in the solution.

5. Theory vs. experiment: comparison and discussion

5.1. Results for KMy solutions at 40 °C

First, we consider the data for KMy solutions at 40 °C without added KCl and HZ. In Fig. 8, the data for conductivity and pH are compared with the theoretical predictions. The kink in conductivity, which corresponds to the CMC, is at c_t = 7.5 mM (Fig. 8a). The data for conductivity below the CMC are fitted by the equation [36]:

$$\kappa = \kappa_0 + \lambda^0 c_t - 204.4 c_t^{3/2} \quad (c_t < \mathrm{CMC}) \tag{5.1}$$

(A = 204.4 mS cm^{-1} M$^{-3/2}$ – see Table 1); here, κ_0 accounts for possible traces of other ionic species, like HCO_3^-, in the used water; this effect is essential only for the lower ionic strengths. The fit yields $\kappa_0 = 0.007 \pm 0.003$ mS/cm; $\lambda^0 \equiv \lambda^0_K + \lambda^0_{My} = 123.6 \pm 0.8$ cm^2 S/mol. Using the known value of λ^0_K, we obtain that the equivalent ionic conductance of My^- ions at 40 °C is $\lambda^0_{My} = 27.9$ cm^2 S/mol, which is listed in Table 1.

For c_t < 7.5 mM, the experimental dependence pH-vs.-c_t (Fig. 8b) agrees very well with a straight line of slope +1. In view of Eq. (3.20), this means that the crystallites in the KMy solutions below the CMC are of myristic acid (HZ). This is confirmed by the plot of the characteristic function f_{HZ} vs. c_t in Fig. 9a. For c_t < 7.5 mM, the plot f_{HZ}-vs.-c_t exhibits a plateau, which gives the solubility product of the myristic acid, $\log K_{HZ} = -11.48$ at 40 °C. The latter value is not much different from the value $\log K_{HZ} = -11.18$ obtained by Lucassen [4] at 20 °C.

At concentrations above the CMC, c_t > 7.5 mM, we used the full procedure for data processing from Section 4.6. In particular, we simultaneously fitted the data for conductivity and pH setting $x = 0$ (no added HZ) and $c_A = 0$ (no added KCl). Three adjustable parameters have been used: the degree of counterion binding to the micelles, θ; the parameter $\omega = n/(j+n)$ that characterizes the stoichiometry of the acid-soap crystallites coexisting with the micelles, and the solubility product of the acid soap, K_{jn}.

The results from the fit of the data for c_t > 7.5 mM (above the CMC) are: $\theta = 0.3$; $\omega = 2/3$ (i.e. 1:2 acid soap coexists with the micelles), and $\log K_{12} = -20.69$. The value of K_{12} predicted by Eq. (3.14) is very close, viz. $\log K_{12} = -21.09$, where the parameter values for 20 °C, given after Eq. (3.10), have been used. The respective theoretical curves, which are shown in Fig. 8a and b, agree very well with the experimental points. As a result of the fit, we determined also the micellization constant in Eq. (4.27): $\log K_{mic} = -2.815$ for KMy at 40 °C.

Having determined all parameters of the model, we can further calculate the concentrations of all species in the solution, including the concentration of myristate molecules incorporated in micelles, $m_Z^{(mic)}$, and in HZ and acid-soap crystallites, m_{HZ} and $m_Z^{(as)}$, assuming that the crystallites are uniformly dispersed in the solution. The results are plotted in Fig. 9b in the form of a concentration diagram. For c_t < CMC, the crystallites are of HZ, whereas for c_t > CMC they are of 1:2 acid soap, i.e. $(HZ)_1(MZ)_2$. In both cases, only a small fraction of the myristate (component Z) exists in the form of crystallites (Fig. 9b). For this reason, for c_t < CMC we have $c_M \approx c_Z$, i.e. the most of the potassium myristate is in the form of M^+ and Z^- ions.

For c_t > CMC, c_M increases, whereas c_Z decreases. This is due to the formation of micelles and follows from Eq. (4.27). For c_t > 100 mM, the concentration of the Z^- monomers is rather low and $c_Z < m_Z^{(as)}$ (Fig. 9b). For c_t > 20 mM, the micelles become the

main component in the solution, which contains the predominant fraction of component Z (the carboxylate).

5.2. Results for KMy solutions at 25 °C

5.2.1. Fits of the data for conductivity and pH

We have already published some results for KMy solutions at 25 °C in relation to the method for analysis of acid-soap stoichiometry proposed in [36]. For this reason, here we first give a brief summary of the results in [36], and then continue with new unpublished results.

For KMy solutions at 25 °C without added KCl and HZ ($c_A = 0$, $x = 0$), the kink in conductivity, which corresponds to the CMC, is at $c_t = 10$ mM. The data for conductivity below the CMC give the equivalent ionic conductance of My^- ions at 25 °C, viz. $\lambda^0_{My} = 20.44\ cm^2\ S/mol$ [36], which is listed in Table 1.

In the concentration region $0.008 < c_t < 1.6$ (mM), the data for pH-vs.-c_t comply with a straight line of slope +1, which indicates that the precipitate in the solution is of myristic acid (HZ) (see Eq. (3.20)). In the concentration region $1.6 < c_t < 10$ (mM), the data for pH-vs.-c_t agree well with a straight line of slope +3, which means that in this region the crystallites in the KMy solutions are of 1:1 acid soap (see Eq. (3.33)). This is confirmed by the plot of the characteristic functions f_{HZ} and f_{11} vs. c_t [36]. The plateaus of these two characteristic functions give $\log K_{HZ} = -11.19$ and $\log K_{11} = -16.8$ in excellent agreement with the values obtained by Lucassen [4], which are given after Eq. (3.10) above.

At concentrations above the CMC, $c_t > 7.5$ mM, the experiment gives pH ≈ 10.67 = const., see the horizontal line in Fig. 2b. The concentration of the K^+ ions, c_M (and the conductivity – see Fig. 2a), increases in this concentration region. Then, to have constant pH, it is necessary the coefficient before $\log(c_M\gamma_\pm)$ in Eq. (4.29) to be equal to zero, i.e. $\omega = \theta$. Therefore, we used the procedure for data processing from Section 4.6 with two adjustable parameters, viz. the degree of counterion binding to the micelles, θ; and the solubility product of the acid soap, K_{jn}. We fitted only the data for conductivity, κ-vs.-c_t, setting $x = 0$ (no added HZ) and $c_A = 0$ (no added KCl). The result of the fit is $\theta = \omega = 0.5$, i.e. 1:1 acid soap crystallites coexist with the micelles [36], and $\log K_{jn} \equiv \log K_{11} = -16.8$, in full agreement with the Lucassen's result for K_{11}.

As a result of the fit, we determined also the micellization constant in Eq. (4.27): $\log K_{mic} = -3.067$ for KMy at 25 °C. The substitution of the obtained values of $\log K_{11}$, $\log K_{mic}$ and $\omega = \theta$ in Eq. (4.29) gives pH 10.67, in excellent agreement with the experimental data for pH in the plateau region (see Fig. 2b).

Having determined all parameters of the model, we calculated the concentrations of all species in the solution, including the concentration of myristate molecules incorporated in micelles, $m_Z^{(mic)}$, and in HZ and acid-soap crystallites, m_{HZ} and $m_Z^{(as)}$. The results are plotted in Fig. 10a. For $c_t < 1.6$ mM, the crystallites are of HZ and their concentration, m_{HZ}, is rather low. For $c_t > 1.6$ mM, the crystallites are of 1:1 acid soap; their stoichiometry does not change at the CMC (at $c_t = 10$ mM). In all cases, only a small fraction of the myristate (component Z) exists in the form of crystallites. For this reason, for $c_t <$ CMC we have $c_M \approx c_Z$, i.e. the most of the potassium myristate is in the form of M^+ and Z^- ions. For $c_t >$ CMC, the amount of the acid soap remains constant and the addition of carboxylate leads to the increase of the micelle concentration (Fig. 10a). For $c_t > 20$ mM the micelles become the main component in the solution, which contains the predominant fraction of component Z (the carboxylate).

5.2.2. The surface tension of KMy solutions

Fig. 10b shows the experimental equilibrium surface tension isotherm, σ-vs.-c_t, for KMy solutions without added KCl and HZ

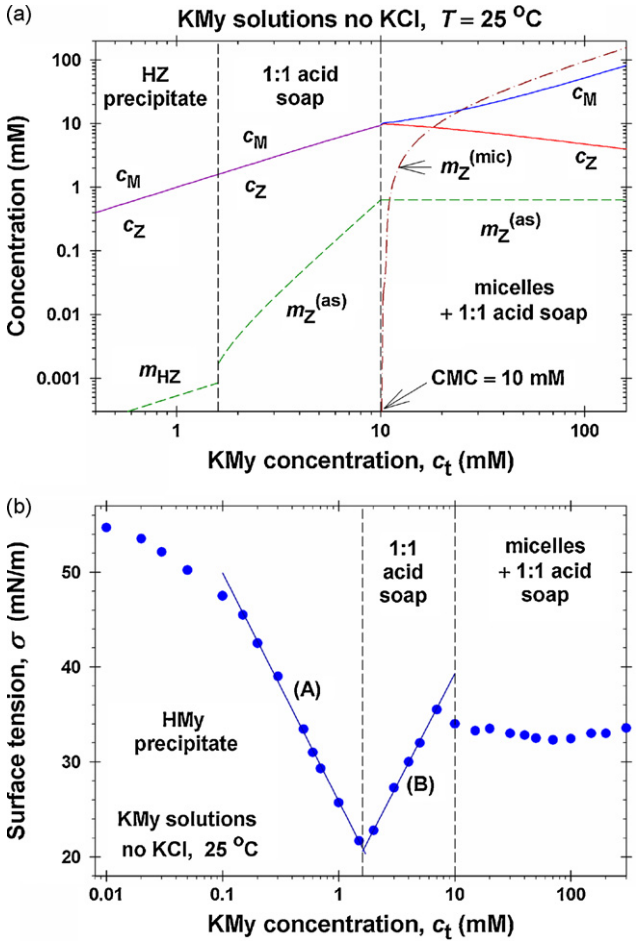

Fig. 10. Results for KMy solutions at 25 °C without added KCl and HZ ($x = 0$). (a) Calculated concentrations of the various species; the concentrations of precipitates, m_{HZ} and $m_Z^{(as)}$, correspond to uniform dispersion of the crystallites in the solution. (b) Experimental data for the surface tension. The vertical dashed lines denote the boundaries between the respective precipitation domains.

($c_A = 0$, $x = 0$) at 25 °C. At concentrations $c_t < 1.6$ mM, including the zone with HZ precipitate (Fig. 10a), σ decreases from 72 down to 22 mN/m. Further, for $1.6 < c_t < 10$ (mM), i.e. in the zone with 1:1 acid-soap precipitate without micelles, the surface tension σ increases. Finally, above the CMC the surface tension remains almost constant, $\sigma \approx 33$ mN/m.

The presence of a region ($1.6 < c_t < 10$ mM), where σ increases with the rise of surfactant concentration, is unusual for the conventional surfactants. The reason for this peculiar behavior is that in this region the adsorption of myristic acid (HZ) is significant, but c_{HZ} decreases with the rise of c_t (see Eqs. (5.10) and (5.11) below). Because we already know the bulk concentrations of all species (Fig. 10a), we can interpret the surface-tension isotherm (Fig. 10b) using the Gibbs adsorption equation:

$$\frac{d\sigma}{kT} = -\tilde{\Gamma}_Z d\ln a_Z - \tilde{\Gamma}_M d\ln a_M - \Gamma_{HZ} d\ln c_{HZ} - \Gamma_{11} d\ln c_{11} \qquad (5.2)$$

Here, Γ_{HZ}, Γ_{11}, $\tilde{\Gamma}_Z$ and $\tilde{\Gamma}_M$ are, respectively, the adsorptions of HZ molecules, 1:1 acid-soap molecules; Z^- ions, and M^+ ions. The tilde symbolizes that the adsorption of the respective ionic species includes a contribution from the diffuse part of the electric double layer; see e.g. reference [41]. $a_Z = c_Z\gamma_\pm$ and $a_M = c_Z\gamma_\pm$ are the bulk activities of the respective ionic species, whereas c_{HZ} and c_{11} are the concentrations of the respective nonionic species; k is the Boltzmann constant, and T is the absolute temperature. Because the solution is electroneutral, the total adsorptions of anions and

cations must be equal: $\tilde{\Gamma}_Z = \tilde{\Gamma}_M$. Then, Eq. (5.2) reduces to:

$$\frac{d\sigma}{kT} = -\tilde{\Gamma}_Z d\ln(a_M a_Z) - \Gamma_{HZ} d\ln c_{HZ} - \Gamma_{11} d\ln c_{11} \quad (5.3)$$

In the *region A* (Fig. 10b), where HZ precipitate is present in the solution, we have $c_{HZ} = S_{HZ} = \text{const.}$, see Eq. (3.16), and consequently the term with Γ_{HZ} in Eq. (5.3) disappears. In addition, the chemical–equilibrium relation for the 1:1 acid-soap molecules is:

$$(a_H a_Z)(a_M a_Z) = Q_{11} c_{11} \quad (5.4)$$

where Q_{11} is an equilibrium constant. Taking log of Eq. (5.4) and differentiating, we obtain:

$$d\ln c_{11} = d\ln(a_M a_Z) \quad (5.5)$$

where the relation $d\ln(a_H a_Z) = d\ln K_{HZ} = 0$ has been also used; see Eq. (3.17). Thus, Eq. (5.3) reduces to:

$$\frac{d\sigma}{kT} = -(\Gamma_{11} + \tilde{\Gamma}_Z) d\ln(a_M a_Z) \quad (5.6)$$

Moreover, in the region A we have $a_Z \approx a_M \approx \gamma_\pm c_t \approx c_t$, compare Fig. 10a and b, and then Eq. (5.6) acquires the form:

$$\frac{d\sigma}{kT} \approx -2(\Gamma_{11} + \tilde{\Gamma}_Z) d\ln c_t \quad (5.7)$$

In view of Eq. (5.7), from the slope of the experimental curve in the region A (Fig. 10b), we determine:

$$\Gamma_{11} + \tilde{\Gamma}_Z = 2.108\ \mu\text{mol/m}^2 \quad (5.8)$$

In the *region B* (Fig. 10b), where 1:1 acid-soap precipitate is present in the solution, we have $c_{11} = \text{const.}$, and consequently the term with Γ_{11} in Eq. (5.3) disappears. Using the chemical–equilibrium relations

$$a_H a_Z = K_A c_{HZ} \quad \text{and} \quad (a_H a_Z)(a_M a_Z) = K_{11} \quad (5.9)$$

see Eqs. (3.9) and (3.32), we derive:

$$d\ln c_{HZ} = d\ln(a_H a_Z) \quad \text{and} \quad d\ln(a_H a_Z) = -d\ln(a_M a_Z) \quad (5.10)$$

The substitution of Eq. (5.10) into Eq. (5.3) yields:

$$\frac{d\sigma}{kT} \approx 2(\Gamma_{HZ} - \tilde{\Gamma}_Z) d\ln c_t \quad (5.11)$$

where the approximation $a_Z \approx a_M \approx \gamma_\pm c_t \approx c_t$ has been used again for $c_t <$ CMC. The positive slope of the σ-vs.-c_t dependence in the region B implies that $\Gamma_{HZ} > \tilde{\Gamma}_Z$. In view of Eq. (5.11), from the slope of the experimental curve in the region B (Fig. 10b), we determine:

$$\Gamma_{HZ} - \tilde{\Gamma}_Z = 2.061\ \mu\text{mol/m}^2 \quad (5.12)$$

For a condensed adsorption monolayer it is natural to assume that its constituent molecules are densely packed:

$$\alpha_{11}\Gamma_{11} + \alpha_{HZ}\Gamma_{HZ} + \alpha_Z\Gamma_Z = 1 \quad (5.13)$$

Here, α_{11}, α_{HZ} and α_Z are the areas per molecule of the respective component at dense packing. In our estimates, we used the following values:

$$\alpha_{HZ} = 22.6\,\text{Å}^2;\ \alpha_Z \approx \alpha_{MZ} = 32.6\,\text{Å}^2;\ \alpha_{11} \approx \alpha_{HZ} + \alpha_{MZ} = 55.2\,\text{Å}^2 \quad (5.14)$$

where the values of α_{HZ} and α_{MZ} are taken from references [23] and [17], respectively. Eqs. (5.8), (5.12) and (5.13) represents a system of three equations for determining the three unknown adsorptions: Γ_{HZ}, Γ_{11} and $\Gamma_Z \approx \tilde{\Gamma}_Z$. The solution of this system yields:

$$\varphi_{HZ} = 0.70;\ \ \varphi_{11} = 0.28 \text{ and } \varphi_Z = 0.02 \quad (5.15)$$

where $\varphi_Y \equiv \alpha_Y \Gamma_Y$ (Y = HZ, 11, Z) are the *area fractions* of the respective components at the interface. Eq. (5.15) means that 70% of the interface is occupied by myristic acid (HZ), 28% by 1:1 acid-soap molecules, and only 2% by myristate anions, Z^-. This result implies that the surface charge density should be rather low. To check this conclusion, we carried out independent experiments with foam films from KMy solutions in the Scheludko–Exerowa cell [42,43]. The interpretation of the measured film thickness by means of the DLVO theory [44,45] gives φ_Z of the order of few percent, in agreement with Eq. (5.15).

5.3. Results for solutions of 87.5 mol% KMy + 12.5 mol% HMy at 25 °C

Here, we consider the data for carboxylate solutions containing 87.5 mol% KMy and 12.5% mol HMy at 25 °C without added KCl. In Fig. 11, the data for conductivity and pH are compared with the theoretical predictions. The kink in conductivity, which corresponds to the CMC, is at c_t = 13 mM (Fig. 11a). (We recall that c_t is the total input concentration of carboxylate, which includes both KMy and HMy.) A second kink is observed at c_t = 2.4 mM, which is better pronounced in the pH plot (Fig. 11b). For $c_t < 2.4$ mM, the data for conductivity are fitted by the equation:

$$\kappa = \kappa_0 + \lambda^0(1-x)c_t - 95.20c_t^{3/2} + 92.72c_t^2 \quad (5.16)$$

where the values of the numerical coefficients are taken from Table 1; the meaning of κ_0 and λ^0 is the same as in Eq. (5.1). The fit yields $\kappa_0 = 0.0023 \pm 0.005$ mS/cm; $\lambda^0 \equiv \lambda^0_K + \lambda^0_{My} = 94.05 \pm 0.9\,\text{cm}^2\,\text{S/mol}$. Using the known value of λ^0_K, we obtain that

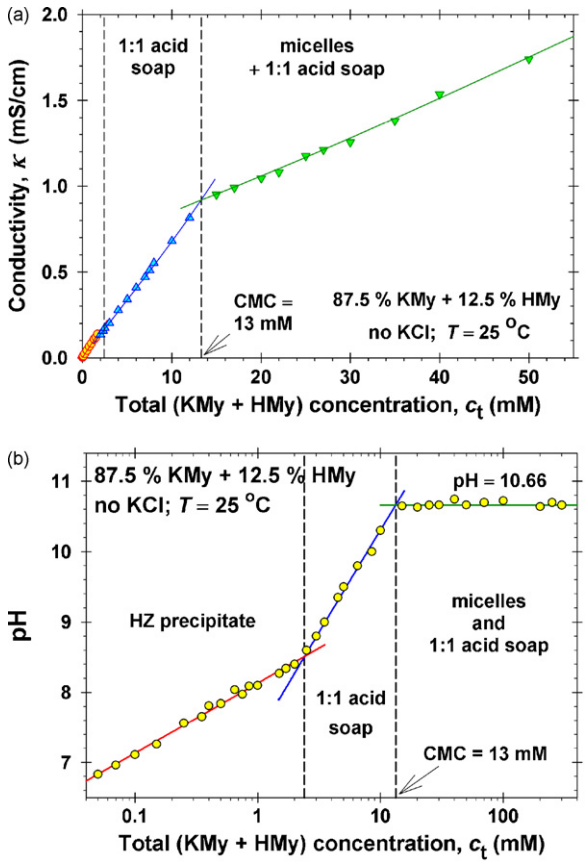

Fig. 11. Results for the conductivity, κ, and pH of solutions of 87.5 mol% KMy and 12.5 mol% HMy at 25 °C. (a) Experimental data for $\kappa(c_t)$ for $c_t \le 50$ mM. The lines are theoretical fits (details in the text). (b) Experimental data and theoretical fits for pH vs. c_t. The vertical dashed lines are the boundaries between zones with different precipitates; c_t is the total input carboxylate concentration due to both KMy and HMy.

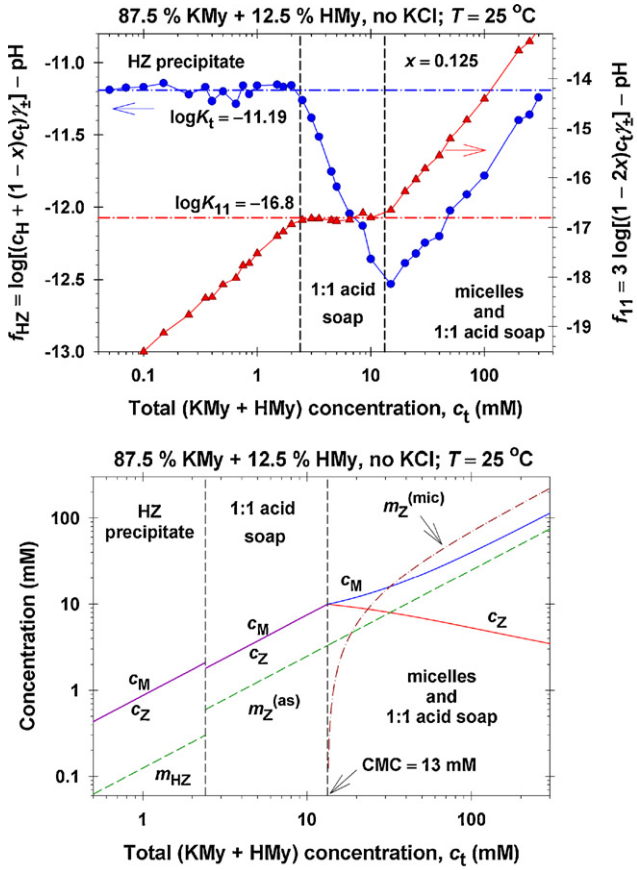

Fig. 12. Results for solutions of 87.5 mol% KMy and 12.5 mol% HMy at 25 °C (no KCl). (a) The characteristic functions $f_{HZ}(c_t)$ and $f_{11}(c_t)$ calculated using the experimental pH(c_t) dependence. (b) Calculated concentrations of the various species; the concentrations of precipitates, m_{HZ} and $m_Z^{(as)}$, correspond to uniform dispersion of the crystallites in the solution.

the equivalent ionic conductance of My^- ions at 25 °C is $\lambda^0_{My} = 20.55\ cm^2\ S/mol$, which is close to the respective value in Table 1.

For $c_t < 2.4$ mM, the experimental dependence pH-vs.-c_t (Fig. 8b) agrees very well with a straight line of slope +1. In view of Eq. (3.20), this means that the crystallites in these solutions are of myristic acid (HZ). Furthermore, for $2.4 < c_t < 13$ mM, the slope of the experimental pH dependence is +3, which implies that the crystalline precipitate is of 1:1 acid soap in this concentration range (see Eq. (3.33)). These conclusions are confirmed by the plot of the characteristic functions f_{HZ} and f_{11} vs. c_t in Fig. 12a. For $c_t < 2.4$ mM, the plot f_{HZ}-vs.-c_t exhibits a plateau, which gives the solubility product of the myristic acid, $\log K_{HZ} = -11.19$, which practically coincides with the value $\log K_{HZ} = -11.18$ obtained by Lucassen [4] at 20 °C. The plateau of $f_{11}(c_t)$, $\log K_{11} = -16.8$, also coincides with the respective value in reference [4] (see Fig. 12a). These results clearly show that the kink in conductivity and pH at $c_t = 2.4$ mM is due to the transition from HZ to 1:1 acid soap precipitate.

At concentrations above the CMC, $c_t > 13$ mM, the experiment gives pH ≈ 10.66 = const. (see Fig. 11b). In such a case, $\omega = \theta$, see Eq. (4.29). For this reason, we used the procedure for data processing from Section 4.6 with two adjustable parameters, viz. θ and K_{jn}. We fitted only the data for conductivity, κ-vs.-c_t, setting $x = 0.125$ (12.5% HZ) and $c_A = 0$ (no added KCl). The result of the fit is $\theta = \omega = 0.5$, i.e. 1:1 acid soap coexist with the micelles [36], and $\log K_{jn} \equiv \log K_{11} = -16.8$, in full agreement with the value of K_{11} independently obtained from our data below the CMC. As a result of the fit, we determined also the micellization constant in Eq. (4.27): $\log K_{mic} = -3.069$, which is practically the same as that obtained in Section 5.2.1, at it should be expected.

Having determined the parameters of the model, we further calculate the concentrations of all species in the solution, including the concentration of myristate molecules incorporated in micelles, $m_Z^{(mic)}$, and in HZ and acid-soap crystallites, m_{HZ} and $m_Z^{(as)}$. The results are plotted in Fig. 12b. Qualitatively, the picture is similar to that in Fig. 10a for KMy without added HZ. The main difference is that the amounts of HZ and acid-soap crystallites, m_{HZ} and $m_Z^{(as)}$, are markedly greater in Fig. 12b in comparison with Fig. 10a. Moreover, in Fig. 12b $m_Z^{(as)}$ increases for $c_t > CMC$, whereas it is constant in Fig. 10a. Both these effects are due to the presence of 12.5% added HZ.

5.4. Solutions of 87.5 mol% KMy + 12.5 mol% HMy + 100 mM KCl at 25 °C

5.4.1. Fits of the data for conductivity and pH

As in the case of solutions of KMy alone, we have already published some results for 87.5 mol% KMy + 12.5 mol% HMy + 100 mM KCl solutions at 25 °C in relation to the method for analysis of acid-soap stoichiometry proposed in [36]. For this reason, here we first give a brief summary of the results in [36], and afterwards continue with new unpublished results.

For the solutions of 87.5 mol% KMy + 12.5 mol% HMy + 100 mM KCl ($x = 0.125$, $c_A = 100$ mM), the kink in pH and conductivity, which corresponds to the CMC, is at $c_t = 5$ mM. For $c_t < 0.4$ mM, the data for pH-vs.-c_t comply with the prediction of Eq. (3.19) with $K_t \approx K_{HZ} = -11.19$, i.e. the precipitate is of myristic acid (HZ). In the concentration region $0.4 < c_t < 5$ (mM), the plot of the characteristic function f_{32} vs. c_t has a plateau, which means that the precipitate is of 3:2 acid soap in this region [36]. The change in the precipitate composition from HZ to $(HZ)_3(MZ)_2$ at $c_t = 0.4$ mM is the reason for the jump in the pH at this concentration (Fig. 4b). Jump in the conductivity κ at $c_t = 0.4$ mM cannot be detected because of the presence of 100 mM background electrolyte (KCl). From the plateau of the experimental plot of f_{32} vs. c_t, we determined the solubility product of the 3:2 acid soap, viz. $\log K_{32} = -47.1$ [36]. On the other hand, Eq. (3.15) predicts $\log K_{32} = -45.6$. The difference could be attributed to effects of non-ideality, insofar as Eq. (3.15) is derived using the assumption that the acid soap is an ideal solid solution [17].

At concentrations above the CMC, $c_t > 5$ mM, we used the full procedure for data processing from Section 4.6. In particular, we simultaneously fitted the data for conductivity and pH setting $x = 0.125$ (12.5% added HZ) and $c_A = 100$ mM. Three adjustable parameters have been used: the degree of counterion binding to the micelles, θ; the parameter $\omega = n/(j+n)$ that characterizes the stoichiometry of the acid-soap crystallites coexisting with the micelles, and the solubility product of the respective acid soap, K_{jn}.

The results from the fit of the data for $c_t > 5$ mM (above the CMC) are: $\theta = 0.6$; $\omega = 2/5$ (i.e. 3:2 acid soap coexists with the micelles), and $\log K_{32} = -47.1$ in full agreement with the value of K_{32} obtained from the pH data below the CMC [36]. In other words, the stoichiometry of the acid-soap precipitate does not change when the micelles appear. As a result of the fit, we determined also the micellization constant in Eq. (4.27): $\log K_{mic} = -3.08$, which is very close to that independently determined in Sections 5.2 and 5.3. Note also that in the present case we have $\omega - \theta \neq 0$, but nevertheless pH ≈ const. above the CMC. In view of Eq. (4.29), this is due to the fact that $a_M \equiv c_M \gamma_\pm \approx$ const. because of the added 100 mM KCl.

Having determined the parameters of the model, we calculated the concentrations of all species in the solution, including the concentration of myristate molecules incorporated in micelles, $m_Z^{(mic)}$, and in HZ and acid-soap crystallites, m_{HZ} and $m_Z^{(as)}$. They are plot-

ted in Fig. 13a in the form of a concentration diagram. Qualitatively, the latter plot is very similar to Fig. 12b. The difference is that the CMC is lowered (from 13 to 5 mM) due to the presence of 100 mM added KCl. For c_t < CMC, the difference $c_M - c_A$, which gives the concentration of M^+ ions dissociated from the KMy, is very close to c_Z, which means that the amount of M^+ ions incorporated into acid-soap precipitates is relatively small. For c_t > 20 mM, the carboxylate (component Z) is contained mostly in the micelles, whereas the amount of carboxylate in the 3:2 acid soap, $m_Z^{(as)}$, is about four times smaller than $m_Z^{(mic)}$ (Fig. 13a).

5.4.2. Surface tension of 87.5 mol% KMy + 12.5 mol% HMy + 100 mM KCl solutions

Fig. 13b shows the experimental equilibrium surface tension isotherm, σ-vs.-c_t, for solutions of 87.5 mol% KMy + 12.5 mol% HMy + 100 mM KCl (x = 0.125, c_A = 100 mM) at 25 °C. At concentrations $c_t \le 0.4$ mM (region A), where HZ precipitate is present (Fig. 13a), σ decreases to 26 mN/m. At $c_t \approx 0.4$–0.5 mM, σ has a jump to ≈36 mN/m. (Note that similar jump is observed in the experimental pH dependence (see Fig. 4b).) Further, for 0.5 < c_t < 5 (mM), i.e. in the zone with 3:2 acid-soap precipitate without micelles, the surface tension σ decreases. Finally, above the CMC the surface tension remains almost constant, $\sigma \approx 30$ mN/m. A possible interpretation of the peculiar behavior of the surface tension of these solutions is the following:

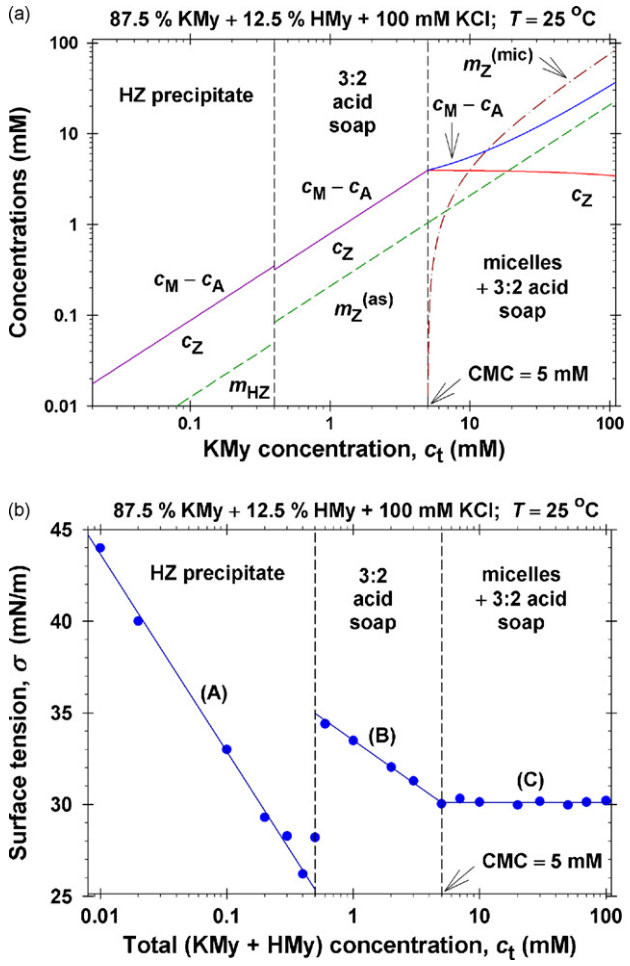

Fig. 13. (a) Calculated concentrations of various species in solutions of 87.5 mol% KMy + 12.5 mol% HMy + 100 mM KCl at 25 °C. (b) Experimental data for the surface tension of these solutions. The vertical dashed lines denote the boundaries between the respective precipitation domains.

In the *region A* (Fig. 13b) we have HZ precipitate and the Gibbs adsorption equation reduces to Eq. (5.6). Because of the added 100 mM KCl, we have $c_M \approx$ const. Moreover, in this region we have $a_Z \approx \gamma_\pm c_t \approx c_t$ (Fig. 13a), and then Eq. (5.6) acquires the form:

$$\frac{d\sigma}{kT} \approx -(\Gamma_{11} + \tilde{\Gamma}_Z) d\ln c_t \tag{5.17}$$

In view of Eq. (5.17), from the slope of the experimental curve in the region A (Fig. 10b), we determine:

$$\Gamma_{11} + \tilde{\Gamma}_Z = 1.888\ \mu mol/m^2 \tag{5.18}$$

Assuming that $\tilde{\Gamma}_Z$ is negligible (see Section 5.2.2), we will use the close-packing relation, Eq. (5.13), in the form:

$$\alpha_{11}\Gamma_{11} + \alpha_{HZ}\Gamma_{HZ} = 1 \tag{5.19}$$

where, as before, $\alpha_{HZ} = 22.6\ Å^2$ and $\alpha_{11} = 55.2\ Å^2$. From Eqs. (5.18) to (5.19), we obtain that in region A the adsorptions are $\Gamma_{11} = 1.888\ \mu mol/m^2$ and $\Gamma_{HZ} = 2.736\ \mu mol/m^2$. In terms of surface area fractions of the adsorbed components, $\varphi_Y \equiv \alpha_Y \Gamma_Y$ (Y = HZ, 11), this result acquires the form:

$$\varphi_{HZ} = 0.37 \text{ and } \varphi_{11} = 0.63 \quad \text{(region A)} \tag{5.20}$$

In other words, in region A 37% of the interface is occupied by myristic acid (HZ), and 63% by 1:1 acid-soap molecules. In comparison with the case without added KCl, Eq. (5.15), the area fraction of the acid soap, φ_{11}, has increased more than twice. A change in this direction was to be expected because of the high K^+ concentration (100 mM) in the present case.

In the *region B* (Fig. 13b), 3:2 acid-soap precipitate is present in the solution (see Fig. 13a). The solubility product for the 3:2 acid soap is:

$$(a_H a_Z)^3 (a_M a_Z)^2 = K_{32} \tag{5.21}$$

Taking log of Eq. (5.21) and differentiating, we derive:

$$d\ln(a_H a_Z) = -\frac{2}{3} d\ln(a_M a_Z) \approx -\frac{2}{3} d\ln c_t \tag{5.22}$$

where we have used that $a_M \approx$ const. because of the added 100 mM KCl, and that $a_Z \approx c_t$ in this concentration range. Next, differentiating Eq. (3.9) and using Eq. (5.22) we obtain:

$$d\ln c_{HZ} = d\ln(a_H a_Z) \approx -\frac{2}{3} d\ln c_t \tag{5.23}$$

Likewise, differentiating Eq. (5.4) and using Eq. (5.22) we obtain:

$$d\ln c_{11} = d\ln(a_H a_Z) + d\ln(a_M a_Z) \approx \frac{1}{3} d\ln c_t \tag{5.24}$$

The substitution of Eqs. (5.23) and (5.24) in the Gibbs adsorption equation, Eq. (5.3), yields:

$$\frac{d\sigma}{kT} \approx -\frac{\Gamma_{11} - 2\Gamma_{HZ}}{3} d\ln c_t \tag{5.25}$$

where the term with $\tilde{\Gamma}_Z$ has been neglected. In view of Eq. (5.25), from the slope of the linear dependence in the region B in Fig. 13(b) we determine:

$$\Gamma_{11} - 2\Gamma_{HZ} = 2.564\ \mu mol/m^2 \tag{5.26}$$

Combining Eqs. (5.19) and (5.26), we obtain that in region B the adsorptions are $\Gamma_{11} = 2.933\ \mu mol/m^2$ and $\Gamma_{HZ} = 0.184\ \mu mol/m^2$. In terms of surface area fractions, $\varphi_Y \equiv \alpha_Y \Gamma_Y$ (Y = HZ, 11) with $\alpha_{HZ} = 22.6\ Å^2$ and $\alpha_{11} = 55.2\ Å^2$, this result acquires the form:

$$\varphi_{11} = 0.97 \text{ and } \varphi_{HZ} = 0.03 \quad \text{(region B)} \tag{5.27}$$

In other words, in region B 97% of the interface is occupied by 1:1 acid soap and only 3% by myristic acid (HZ). In other words, in region B the interface is almost entirely occupied by 1:1 acid soap. Note that in the region B we have 3:2 acid-soap precipitate in the bulk,

Table 2
Comparison of results for the four investigated systems.

System (°C)	T (°C)	Region with HZ precipitate	Region with j:n acid soap	CMC (mM)	Micelles coexist with j:n acid soap
KMy	40	c_t < 7.5 mM	–	7.5	j:n = 1:2; θ = 0.3; $\log K_{mic} = -2.82$
KMy	25	c_t < 1.6 mM	1.6 – 10 mM, j:n = 1:1	10	j:n = 1:1; θ = 0.5; $\log K_{mic} = -3.07$
87.5% KMy + 12.5 % HZ	25	c_t < 2.4 mM	2.4 – 13 mM, j:n = 1:1	13	j:n = 1:1; θ = 0.5; $\log K_{mic} = -3.07$
87.5% KMy + 12.5 % HZ + 100 mM KCl	25	c_t < 0.4 mM	0.4 – 5 mM, j:n = 3.2	5	j:n = 3:2; θ = 0.6; $\log K_{mic} = -3.08$

which is the reason for the decrease of the surface tension, σ, in this region. Indeed, if the soap were of 1:1 type simultaneously in the bulk and at the surface, then σ would be constant because the presence of precipitate would fix the chemical potential of the 1:1 acid-soap complex.

Finally, in the region C (Fig. 13b), i.e. above the CMC, the micelles coexist with 3:2 acid soap. Consequently, Eqs. (4.27) and (5.21) are simultaneously fulfilled, and in addition $a_M \approx$ const. because of the added 100 mM KCl. The latter three equations fix the values of a_H, a_M and a_Z, and then the Gibbs adsorption equation implies $\sigma \approx$ const. in agreement with the data in region C (Fig. 13b).

5.5. Comparison of results for the different systems

Results for the four investigated systems are compared in Table 2. At the lower concentrations, all systems contain myristic acid (HZ) precipitate. With the further increase of c_t, the HZ precipitate is replaced by acid-soap precipitate. The latter appears at lower carboxylate concentrations when KCl is added (the last row of Table 2). The rise of temperature and KCl concentration leads to lower CMC. At temperature 25 °C, the type of the acid soap is the same below and above the CMC. At temperature 40 °C, acid soap is absent below the CMC and 1:2 acid soap is present above the CMC. The degree of counterion binding to the micelles is lower at 40 °C, θ = 0.3; it is the highest in the presence of 100 mM added KCl, θ = 0.6. The values of the micellization constant at 25 °C, determined independently for the three investigated systems, are practically coinciding, $-\log K_{mic}$ = 3.07–3.08, which confirms the adequacy of the used theoretical model. The value obtained at 40 °C is only slightly smaller, viz. $-\log K_{mic}$ = 2.82.

At 25 °C it was possible to collect sufficient amounts of acid-soap crystallites from the solutions by filtration. Further, these crystallites were subjected to analysis to determine their stoichiometry, j:n. The used procedures and the obtained results are described in reference [36]. In all investigated cases, the results for j:n from this independent analysis coincide with the results obtained in the present article on the basis of interpretation of pH and conductivity data; see Table 2 in reference [36].

As seen in Table 2, acid-soap crystallites of 1:2, 1:1 and 3:2 stoichiometries have been identified in the investigated systems. The interactions that govern the acid-soap stoichiometry are (i) the formation of a hydrogen bond between the fatty acid (HZ) and neutral soap (MZ) molecules, and (ii) the different possible ways of coordination of the alkaline ion (in our case K^+) with the carboxylate oxygen atoms; see e.g. ref. [3].

6. Summary and conclusions

In the present study, we carried out parallel pH, conductivity, and solubilization measurements, which indicate that micelles are present in KMy solutions at the higher concentrations (Figs. 2 and 4), in contrast with the results for NaMy, where no micelles were detected at 25 °C (see Fig. 1 and reference [17]). The direct observations show that crystallites are present in the micellar solutions (Figs. 3 and 4). Theoretical expressions describing the concentration dependences of conductivity and pH of the solutions that contain coexisting micelles and crystallites are derived (Section 4). By comparison of theory and experiment, for each specific system we determined the micelle charge and the stoichiometry of the soap crystallites. Diagrams showing concentrations of all species in the solution, are built up (Figs. 9b, 10a, 12b and 13a).

The comparison of theory and experiment indicates that the undissociated fatty acid, HZ, is incorporated in acid-soap crystallites, i.e. HZ behaves as initiator of crystallization. The rest of dissolved carboxylate, MZ, forms micelles that are composed only of carboxylate anions, Z^-, and bound counterions, M^+. Above 2–3 times the CMC, the main mass of the carboxylate is in micellar form, despite the presence of coexisting acid-soap crystallites (see Figs. 9b, 10a, 12b and 13a).

Surface tension isotherms are obtained and interpreted knowing the bulk concentrations of the species in the solutions. The adsorption layer is composed mostly of 1:1 acid soap and HZ, the adsorption of Z^- (and the surface charge) being low, c.a. 1% (see Figs. 10b and 13b), and the related text. Not only the appearance of micelles, by also the change in the stoichiometry of the acid soaps in the solution leads to kinks, and even jumps (Fig. 13b), in the surface tension isotherm.

The results for acid-soap stoichiometry j:n, obtained here from the data for pH and κ vs. c_t, have been verified by independent analysis of crystals collected from the solutions [36]. In all investigated cases, the two methods give coinciding results [36].

Acknowledgements

We gratefully acknowledge the support of Unilever Research & Development, Trumbull, Connecticut, and of EU COST Action D43 for this study. The authors are thankful to Dr. N.C. Christov for his cooperation in electrolytic conductivity measurements.

References

[1] M.R. Porter, Handbook of Surfactants, Blackie Academic & Professional, London, 1997, p. 100.
[2] R.G. Bartolo, M.L. Lynch (Eds.), Kirk-Othmers Encyclopedia of Chemical Technologies, fourth ed., Wiley, New York, 1997.
[3] M.L. Lynch, F. Wireko, M. Tarek, M. Klein, Intermolecular interactions and the structure of fatty acid–soap crystals, J. Phys. Chem. B 105 (2001) 552–561.
[4] J. Lucassen, Hydrolysis and precipitates in carboxylate soap solutions, J. Phys. Chem. 70 (1966) 1824–1830.
[5] P. Ekwall, W. Mylius, Über saure Natriumsalze der Palmitinsäure, Ber. Deutschen Chem. Gesell. 62 (1929) 1080–1084.
[6] P. Ekwall, W. Mylius, Über saure Natriumsalze der Laurinsäure, Ber. Deutschen Chem. Gesell. 62 (1929) 2687–2690.
[7] J.W. McBain, M.C. Field, Phase rule equilibria of acid soaps. I. Anhydrous acid potassium laurate, J. Phys. Chem. 37 (1933) 675–684.
[8] J.W. McBain, M.C. Field, Phase rule equilibria of acid soaps. II. Anhydrous acid sodium palmitates, J. Chem. Soc. (1933) 920–924, doi:10.1039/JR9330000920.
[9] P. Ekwall, Solutions of alkali soaps and water in fatty acids, Colloid Polym. Sci. 266 (1988) 279–282.
[10] M.L. Lynch, Y. Pan, R.G. Laughlin, Spectroscopic and thermal characterization of 1:2 sodium soap/fatty acid acid–soap crystals, J. Phys. Chem. 100 (1996) 357–361.
[11] M.L. Lynch, Acid–soaps, Curr. Opin. Colloid Interface Sci. 2 (1997) 495–500.
[12] X. Wen, E.I. Franses, Effect of protonation on the solution and phase behavior of aqueous sodium myristate, J. Colloid Interface Sci. 231 (2000) 42–51.
[13] X. Wen, J. Lauterbach, E.I. Franses, Surface densities of adsorbed layers of aqueous sodium myristate inferred from surface tension and infrared reflection absorption spectroscopy, Langmuir 16 (2000) 6987–6994.
[14] J.R. Kanicky, D.O. Shah, Effect of premicellar aggregation on the pKa of fatty acid soap solutions, Langmuir 19 (2003) 2034–2038.
[15] M. Heppenstall-Butler, M.F. Butler, Nonequilibrium behavior in the three-component system stearic acid–sodium stearate–water, Langmuir 19 (2003) 10061–10072.

[16] S. Zhu, M. Heppenstall-Butler, M.F. Butler, P.D.A. Pudney, D. Ferdinando, K.J. Mutch, Acid soap and phase behavior of stearic acid and triethanolamine stearate, J. Phys. Chem. B 109 (2005) 11753–11761.
[17] P.A. Kralchevsky, K.D. Danov, C.I. Pishmanova, S.D. Kralchevska, N.C. Christov, K.P. Ananthapadmanabhan, A. Lips, Effect of the precipitation of neutral-soap, acid-soap and alkanoic-acid crystallites on the bulk pH and surface tension of soap solutions, Langmuir 23 (2007) 3538–3553.
[18] Yu.B. Vysotsky, D.V. Muratov, F.L. Boldyreva, V.B. Fainerman, D. Vollhardt, R. Miller, Quantum chemical analysis of the thermodynamics of 2D cluster formation of *n*-carboxylic acids at the air/water interface, J. Phys. Chem. B 110 (2006) 4717–4730.
[19] Yu.B. Vysotsky, E.A. Belyaeva, D. Vollhardt, E.V. Aksenenko, R. Miller, Simplified method of the quantum chemical analysis for determination of thermodynamic parameters of 2D cluster formation of amphiphilic compounds at the air/water interface, J. Colloid Interface Sci. 326 (2008) 339–346.
[20] V.M. Kaganer, H. Möhwald, P. Dutta, Structure and phase transitions in Langmuir monolayers, Rev. Mod. Phys. 71 (1999) 779–819.
[21] J.G. Petrov, T. Pfohl, H. Möhwald, Ellipsometric chain length dependence of fatty acid Langmuir monolayers. A heads-and-tails model, J. Phys. Chem. B 103 (1999) 3417–3424.
[22] B.D. Casson, C.D. Bain, Unequivocal evidence for a liquid–gas phase transition in monolayers of decanol adsorbed at the air/water interface, J. Am. Chem. Soc. 121 (1999) 2615–2616.
[23] K.D. Danov, P.A. Kralchevsky, K.P. Ananthapadmanabhan, A. Lips, Interpretation of surface-tension isotherms of n-alkanoic (fatty) acids by means of the van der Waals model, J. Colloid Interface Sci. 300 (2006) 809–813.
[24] K. Golemanov, N.D. Denkov, S. Tcholakova, M. Vethamuthu, A. Lips, Surfactant mixtures for control of bubble surface mobility in foam studies, Langmuir 24 (2008) 9956–9961.
[25] K. Golemanov, S. Tcholakova, N.D. Denkov, K.P. Ananthapadmanabhan, A. Lips, Breakup of bubbles and drops in steadily sheared foams and concentrated emulsions, Phys. Rev. E 78 (2008) 051405.
[26] A. Chatterjee, S. Maiti, S.K. Sanyal, S.P. Moulik, Micellization and related behaviors of *n*-cetyl-*n*-ethanolyl-*n*,*n*-dimethyl and *n*-cetyl-*n*,*n*-diethanolyl-*n*-methyl ammonium bromide, Langmuir 18 (2002) 2998–3004.
[27] M.S. Bakshi, A. Kaura, J.D. Miller, V.K. Paruchuri, Sodium dodecyl sulfate–poly(amidoamine) interactions studied by AFM imaging, conductivity, and Krafft temperature measurements, J. Colloid Interface Sci. 278 (2004) 472–477.
[28] C. Vautier-Giongo, H.O. Pastore, Micellization of CTAB in the presence of silicate anions and the exchange between bromide and silicate at the micelle surface, J. Colloid Interface Sci. 299 (2006) 874–882.
[29] P.D. Todorov, G.S. Marinov, P.A. Kralchevsky, N.D. Denkov, P. Durbut, G. Broze, A. Mehreteab, Kinetics of triglyceride solubilization by micellar solutions of nonionic surfactant and triblock copolymer: 3. Experiments with single drops, Langmuir 18 (2002) 7896–7905.
[30] P.D. Todorov, P.A. Kralchevsky, N.D. Denkov, G. Broze, A. Mehreteab, Kinetics of solubilization of *n*-decane and benzene by micellar solutions of sodium dodecyl sulfate, J. Colloid Interface Sci. 245 (2002) 371–382.
[31] P.A. Kralchevsky, N.D. Denkov, Triblock copolymers as promoters of solubilization of oils in aqueous surfactant solutions, in: Pu Chen (Ed.), Molecular Interfacial Phenomena of Polymers and Biopolymers, Woodhead Publication, Cambridge, UK, 2005, pp. 538–579 (Chapter 15).
[32] R.A. Robinson, R.H. Stokes, Electrolyte Solutions, second ed., Dover Publications, New York, 2002.
[33] M.L. Corrin, W.D. Harkins, The effect of salts on the critical concentration for the formation of micelles in colloidal electrolytes, J. Am. Chem. Soc. 69 (1947) 683–688.
[34] M. Bourrel, R.S. Schechter, Microemulsions and Related Systems, M. Dekker, New York, 1988, pp. 48–53.
[35] H.S. Harned, B.B. Owen, The Physical Chemistry of Electrolytic Solutions, second ed., Reinhold Publishing Corp., New York, 1950.
[36] P.A. Kralchevsky, M.P. Boneva, K.D. Danov, K.P. Ananthapadmanabhan, A. Lips, Method for analysis of the composition of acid soaps by electrolytic conductivity measurements, J. Colloid Interface Sci. 327 (2008) 169–179.
[37] F. Kohlrausch, On the conductivity of electrolytes dissolved in water in relation to the migration of their components, Paper Presented before the Göttingen Academy of Sciences, May 6, 1876.
[38] A.A. Ravdel, A.M. Ponomareva (Eds.), Concise Handbook of Physiochemical Quantities, eight ed., Khimiya, Leningrad, 1983, pp. 120–121 (in Russian).
[39] J.N. Israelachvili, Intermolecular and Surface Forces, second ed., Academic Press, London, 1992, p. 110.
[40] R.C. Weast (Ed.), CRC Handbook of Chemistry and Physics, CRC Press, Boca Raton, FL, 2000.
[41] P.A. Kralchevsky, K.D. Danov, G. Broze, A. Mehreteab, Thermodynamics of ionic surfactant adsorption with account for the counterion binding: effect of salts of various valency, Langmuir 15 (1999) 2351–2365.
[42] A. Scheludko, D. Exerowa, Über den elektrostatischen Druck in Schaumfilmen aus wässerigen Elektrolytlösungen, Kolloid-Z 165 (1959) 148–151.
[43] A. Scheludko, Thin liquid films, Adv. Colloid Interface Sci. 1 (1967) 391–464.
[44] B.V. Derjaguin, L.D. Landau, Theory of stability of highly charged lyophobic sols and adhesion of highly charged particles in solutions of electrolytes, Acta Physicochim. USSR 14 (1941) 633–652.
[45] E.J.W. Verwey, J.Th.G. Overbeek, Theory of Stability of Lyophobic Colloids, Elsevier, Amsterdam, 1948.